AD NUMBER

816 189

CLASSIFICATION CHANGES

TO

FROM

AUTHORITY

WRDC 1 Ist LTR d+d 21 MAR 89
(For Entries 11 thru)

AFML-TR-65-2
PART I, VOLUME XI

TERNARY PHASE EQUILIBRIA IN TRANSITION METAL-BORON-CARBON-SILICON SYSTEMS

PART I. RELATED BINARY SYSTEMS
VOLUME XI. FINAL REPORT ON THE Mo-C SYSTEM

E. RUDY
ST. WINDISCH
A. J. STOSICK
J. R. HOFFMAN

AEROJET-GENERAL CORPORATION

TECHNICAL REPORT No. AFML-TR-65-2, PART I, VOLUME XI

APRIL 1967

AIR FORCE MATERIALS LABORATORY
RESEARCH AND TECHNOLOGY DIVISION
AIR FORCE SYSTEMS COMMAND
WRIGHT-PATTERSON AIR FORCE BASE, OHIO

NOTICES

When Government drawings, specifications, or other data are used for any purpose other than in connection with a definitely related Government procurement operation, the United States Government thereby incurs no responsibility nor any obligation whatsoever; and the fact that the Government may have formulated, furnished, or in any way supplied the said drawings, specifications, or other data, is not to be regarded by implication or otherwise as in any manner licensing the holder or any other person or corporation, or conveying any rights or permission to manufacture, use, or sell any patented invention that may in any way be related thereto.

Copies of this report should not be returned to the Research and Technology Division unless return is required by security considerations, contractual obligations, or notice on a specific document.

400 - May 1967 - CO192 - 34-843

TERNARY PHASE EQUILIBRIA IN TRANSITION METAL-BORON-CARBON-SILICON SYSTEMS

PART I. RELATED BINARY SYSTEMS
VOLUME XI. FINAL REPORT ON THE Mo-C SYSTEM

E. RUDY
ST. WINDISCH
A. J. STOSICK
J. R. HOFFMAN

FOREWORD

The research described in this report was carried out at the Materials Research Laboratory, Aerojet-General Corporation, Sacramento, California, under USAF Contract No. AF 33(615)-1249. The contract was initiated under Project No. 7350, Task No. 735001, and was administered under the direction of the Air Force Materials Laboratory, Research and Technology Division, with Lt. P. J. Marchiando acting as Project Engineer, and Dr. E. Rudy, Aerojet-General Corporation, as Principal Investigator. Professor Dr. Hans Nowotny, University of Vienna, Served as Consultant to the project.

The project, which includes the experimental and theoretical investigations of ternary and related binary systems in the system classes Me_1-Me_2-C, Me-B-C, Me_1-Me_2-B, Me-Si-B, and Me-Si-C, was initiated on 1 January 1964.

The present report summarizes the investigations in the binary molybdenum-carbon system. A unabridged version of the present report has been submitted for publication in the Transactions of the AIME.

The authors wish to acknowledge the help of Messrs. J. Pomodoro and R. Cobb during the course of the experimental work; Mr. W. E. Trahan, Quality Control Division of Aerojet-General Corporation, for supervising the chemical analytical work, Mr. R. Cristoni for the preparation of the illustrations, and Mrs. J. Weidner for typing the report.

The manuscript of this report was released by the authors in January, 1967 for publication as an RTD Technical Report.

Other reports issued under USAF Contract AF 33(615)-1249 have included:

Part I.	Related Binaries	
	Volume I.	Mo-C System
	Volume II.	Ti-C and Zr-C Systems
	Volume III.	Systems Mo-B and W-B
	Volume IV.	Hf-C System
	Volume V.	Ta-C System. Partial Investigations in the Systems V-C and Nb-C
	Volume VI.	W-C System. Supplemental Information on the Mo-C System
	Volume VII.	Ti-B System
	Volume VIII.	Zr-B System
	Volume IX.	Hf-B System
	Volume X.	V-B, Nb-B, and Ta-B Systems
Part II.	Ternary Systems	
	Volume I.	Ta-Hf-C System
	Volume II.	Ti-Ta-C System
	Volume III.	Zr-Ta-C System

	Volume IV.	Ti-Zr-C, Ti-Hf-C, and Zr-Hf-C Systems
	Volume V.	Ti-Hf-B System
	Volume VI.	Zr-Hf-B System
	Volume VII.	Systems Ti-Si-C, Nb-Si-C, and W-Si-C
	Volume VIII.	Ta-W-C System
	Volume IX.	Zr-W-B System. Pseudo-binary System TaB_2-HfB_2
	Volume X.	Systems Zr-Si-C, Hf-Si-C, Zr-Si-B, and Hf-Si-B
	Volume XI.	Systems Hf-Mo-B and Hf-W-B
	Volume XII.	Ti-Zr-B System
Part III.	Special Experimental Techniques	
	Volume I.	High Temperature Differential Thermal Analysis
	Volume II.	A Pirani-Furnace for the Precision Determination of the Melting Temperatures of Refractory Metallic Substances.
Part IV.	Thermochemical Calculations	
	Volume I.	Thermodynamic Properties of Group IV, V, and VI Binary Transition Metal Carbides.
	Volume II.	Thermodynamic Interpretation of Ternary Phase Diagrams
	Volume III.	Computational Approaches to the Calculation of Ternary Phase Diagrams.

This technical report has been reviewed and is approved.

W. G. RAMKE
Chief, Ceramics and Graphite Branch
Metals and Ceramics Division
Air Force Materials Laboratory

ABSTRACT

The binary alloy system molybdenum-carbon was investigated by means of X-ray, metallographic, thermoanalytical, and melting point techniques on chemically analyzed specimens. The system (Figure 39) is characterized by three congruently melting, intermediate phases, Mo_2C, η-MoC_{1-x}, and α-MoC_{1-x}, of which only Mo_2C is stable at temperatures below 1650°C. Substoichiometric (< 32.5 At% C) dimolybdenum carbide undergoes a homogeneous sublattice order-disorder transformation at temperatures of approximately 1400°C, whereas hyperstoichiometric compositions undergo a discontinuous phase-change. The order-disorder transitions in the Me_2C phases are discussed in terms of the structural changes involved in the transformation processes and the absence of long range sublattice coherency in stoichiometric or hyperstoichiometric compositions attributed to the impossibility of obtaining long range order in a linear chain of alternating carbon atoms and vacancies.

From the experimental phase relationships and the known thermodynamic data for Mo_2C, limits for the free energies of formation for the high temperature phases η-MoC_{1-x} and α-MoC_{1-x} are derived and found to be in good agreement with data previously obtained from phase equilibria in ternary metal-carbon systems.

TABLE OF CONTENTS

LIST OF ILLUSTRATIONS

LIST OF ILLUSTRATIONS (Cont'd)

LIST OF ILLUSTRATIONS (Cont'd)

LIST OF TABLES

I. INTRODUCTION AND SUMMARY OF PREVIOUS WORK

In the course of studies of the high temperature phase relationships in ternary systems of refractory transition metals with carbon[1], a number of inconsistencies found in previous work necessitated a reexamination of some of the related metal-carbon binaries. A reassessment of the binary system data also seemed to be desirable, because the thermodynamic evaluation of the phase equilibria in certain ternary metal-carbon systems pointed to the existence of sublattice disordering reactions in the Me_2C-Phase[2] at high temperatures. In the meantime, the occurrence of these order-disorder transformations had been ascertained by differential-thermoanalytical techniques[3], although the reactions were not investigated in closer detail at that time.

In the molybdenum-carbon system, the existence of at least three intermediate phases, Mo_2C, η-MoC_{1-x}, and α-MoC_{1-x}, of which the latter two are stable at high temperatures only, is known from previous work and the structures of these phases are established[4] (Table 1). There is general agreement, that the solubility of carbon in molybdenum is small[4].

Dimolybdenum carbide, with a hexagonal close-packed arrangement of metal atoms[4, 13], is only pseudohexagonal; the ordered distribution of the carbon atoms requires the adoption of an orthorhombic cell, whose dimensions are related to the hexagonal cell dimensions by $a_{o.r.} = c_{hex}$; $b_{o.r.} = 2a_{hex}$; and $c_{o.r.} = a_{hex}\sqrt{3}$ [8].

The structure of the hexagonal η-MoC_{1-x} is closely related to the B1-type[9]. The phase occurs in the concentration range from 38 to 40 At% C[10, 14] and was reported to decompose at 1450 ± 100°C into Mo_2C and graphite[15].

The cubic (B1) α-MoC_{1-x}[10, 11] is also a high temperature phase and can be obtained in pure form only by severe quenching from temperatures above 2000°C[10], or by rapid cooling under pressure[11]. A

Table 1. Structure and Lattice Parameters of Molybdenum Carbides

Phase	Structure	Lattice Parameters, Å
Mo_2C	hex., L'3-type	a=3.00 to 3.012 (5,6) c=4.732 to 4.735 a=3.0028 at MoC (7) c=4.7288
	orthorh. D_{2h}^{14}	a_o=7.24$_4$; b_o=6.004, c_o=5.19$_9$ (8)*
η-MoC_{1-x}	hex., D_{6h}^{4}	a=3.006 (9) a=3.013 at $MoC_{\sim 2/3}$ (10) c=14.61 c=14.64
α-MoC_{1-x}	cub., B1-type	a=4.27 (11) c=4.281 (10)
γ-MoC**	hex., WC-type	a=2.898 (12) c=2.809
γ'-MoC**	hex., $P6_3/mmc$	a=2.932 (12) c=10.97

* The orthorhombic axes of the Mo_2C-order structure are related to the hexagonal cell by: $a_o = c_{hex}$; $b_o = 2a_{hex}$; $c_o = a_{hex}\sqrt{3}$

** Probably oxygen-stabilized phases.

decomposition temperature of approximately 2000°C was estimated from thermodynamic calculations[10, 14], but recent investigations by T.C. Wallace et al.[15] indicate temperatures above 2100°C. The phase exists only at a carbon defect of approximately 10 atomic percent[10, 14].

J.L. Lander and L.H. Germer[16] claimed to have found a cubic Mo_2C in the reaction products of molybdenum carbonyl-steam mixtures. A

carbide having the tungsten monocarbide structure[5, 12] (γ-MoC) was said to be unstable below 700°C[17], whereas another hexagonal monocarbide (γ'-MoC, space group $P6_3/mmc$) was reported to result from the low temperature carburization of molybdenum[12]. The suppositions of R. Kieffer and F. Benesovsky[4], attributing the appearance of these phases due to oxygen stabilization, seem to receive support from a recent observation of oxycarbides of corresponding structure by I. F. Ferguson et al.[18]

On the metal-rich side of the system, a eutectic between Mo and Mo_2C is formed at 2200°C[19, 20] and 12.8 At% C[19]. T. Takei[21] places the eutectic composition at 25 At% carbon.

Dimolybdenum carbide forms in a peritectic reaction at temperatures near 2400°C[15, 19, 20, 22]. Other measurements of the maximum solidus temperature for this phase yielded 2230-2330°C[23], and 2690 $\pm$ 50°C[24]. The monocarbide was said to melt congruently at 2570°C[23] and 2650°C[9, 24], respectively; however, according to T. C. Wallace et al.[15], the stoichiometric composition melts heterogeneously at 2575°C. A eutectic MoC + C was reported at approximately 2400°C and 70 At% C[4, 9], but a peritectic isotherm at 2560°C also was proposed[25].

II. EXPERIMENTAL

A. STARTING MATERIAL AND ALLOY PREPARATION

The elemental powders, as well as a specially prepared master alloy of Mo_2C, served as the starting materials for the preparation of all other experimental alloy samples. The molybdenum powder (Wah Chang Corporation, Albany, Oregon) had the following major impurities (contents in ppm): O-1120, Si-<200, N-60, C-140, Fe-<20, Ni-40, Co-50, sum of other metallic impurities (Al, Cr, Cu, Mg, Mn, Pb, Sn, W. Ti)-<600. The overall purity of this starting material was better than 99.75%. A lattice parameter of 3.147$_3$ Å was obtained from a Cu-K_α powder pattern.

The Mo_2C master alloy was prepared by reacting the carefully blended and cold-compacted mixtures of molybdenum and carbon for 2 hours at 1600 to 1900°C under a vacuum of $<10^{-4}$ Torr in a graphite element furnace. The reaction lumps were crushed and ball-milled under carbon tetrachloride to a grain size below 60 microns. The powder slurry was then centrifuged, the resulting cake washed, and traces of cobalt-pickup from the carbide-lined ball mill jars were removed by leaching in a hot 8N mixture of sulfuric and hydrochloric acid. The resulting product had a total carbon content of 32.7 $\pm$ 0.2 At%, of which 0.2 At% were present in elemental form. Other contaminants included (in ppm): O-70, N-<10, Si-<100, sum of other impurities-<700.

The spectrographic grade graphite powder was purchased from Union Carbide Corporation, Carbon Products Division. The total impurity content was below 2 ppm, and lattice parameters of a=2.463 Å, and c=6.729 Å were obtained from an exposure with Cu-K radiation.

The majority of the experimental alloys were prepared by short-duration (2 to 5 minutes) hot pressing[26] of the carefully blended powder mixtures in graphite dies. The temperatures employed generally varied between 1650 to 2100°C. After hot pressing, the surface reaction zone, which typically was approximately 0.2 mm thick, was removed by grinding, and the uncontaminated core of the alloy samples subjected to prehomogenization treatments at 1800 and 1500°C in a tungsten mesh element furnace (R. Brew Company) under a vacuum of better than 5×10^{-5} Torr. One piece of each alloy was also arc-melted. The prehomogenized alloys were then analyzed and used as stock material for the further studies. A limited number of samples, mainly for melting point and DTA-studies on excess molybdenum-containing alloys, was also prepared by cold-pressing and subsequent sintering of the compacts at 1600°C under vacuum.

B. DETERMINATION OF MELTING TEMPERATURES

The solidus temperatures of the alloys were determined using the method devised by M. Pirani and H. Alterthum[27]. In this technique, a small sample bar with a black body hole in the center is heated resistively

between two water-cooled electrodes to the temperature of the phase change. The temperature of the sample is measured optically with a disappearing-filament type micropyrometer through a quartz window in the furnace wall. A small hole, in the order of 0.6 to 1.0 mm in diameter and 4 to 6 mm deep, drilled or pressed into the sample, serves as the reference point for the temperature measurements. Design details of the apparatus used in this laboratory, as well as calibration procedures for the temperature measuring instruments and the determination of the correction factors to be applied for the quartz window are reported elsewhere[28] and need therefore not be treated in any length here.

In the measurements of molybdenum-carbon alloys, the specimens were held under slight compression (~ 200 gms) between the water-cooled copper electrodes, and heated under vacuum to temperatures between 1800 to 2000°C. The samples were held at this temperature until the vacuum stabilized and no further degassing was noticeable. The furnace chamber was then pressurized to approximately tw atmospheres with high purity helium and the temperature of the specimen was slowly raised until melting occurred. Apart from a few initial runs under vacuum, where carbon losses between two and five atomic percent in the melted zone were encountered, the analyzed carbon contents after melting agreed, as a rule, within one atomic percent with the nominal concentrations.

Contamination of the as-melted alloys by oxygen typically was less than 60 ppm and its possible effect upon the phase relationships will therefore be disregarded in the discussion of the experimental results.

In order to separate the relative accuracies obtained in the temperature measurements from the calibration errors and the temperature uncertainties in the calibration standard, the temperature figures in the text, unless otherwise designated, refer to the reproducibility of the measurements. To obtain the overall temperature error limits, the standard deviations in the measurements (σ_m) have to be combined with the calibration errors (σ_c) according to

$$\sigma_{tot} = \pm\sqrt{\sigma_c^2 + \sigma_m^2}$$

Representative values for the calibration uncertainties, σ_c, for our instruments are given in Table 2.

Table 2. Temperature Uncertainties for the Micro-Optical Pyrometers (~90% Confidence Level).

Temperature, °C	Uncertainty ± °C
1100	4
2000	7
2300	8
3000	10
3600	25

C. DIFFERENTIAL AND DERIVATIVE THERMAL ANALYSIS[3]

Using graphite and tantalum monocarbide as comparison standards, and using graphite as container for the specimens, the differential thermal behavior of approximately 30 different alloy compositions was studied. Alloys containing less than 33 atomic percent carbon carburized rather rapidly above 2000°C, and therefore, for these compositions, the container walls were lined with tantalum carbide to keep the interaction at a tolerable level. Each sample was studied at heating and cooling rates varying between 0.5°C and 18°C per second. The temperatures of the thermal arrests were detected by an infrared radiation thermometer and were independently measured with a disappearing filament type micropyrometer sighting through a separate quartz port in the furnace.

In addition to the DTA-measurements as described above, additional derivative thermal analytical studies were carried out in another unit, which essentially eliminates the problems arising from the interaction between the test specimen and the container material[29]. In this setup, a bar-shaped specimen is heated resistively in the melting point furnace and the temperatures are measured photoelectrically through the quartz port from outside the furnace. The principle of operation of the radiation detection part of the system is shown in Figure 1.

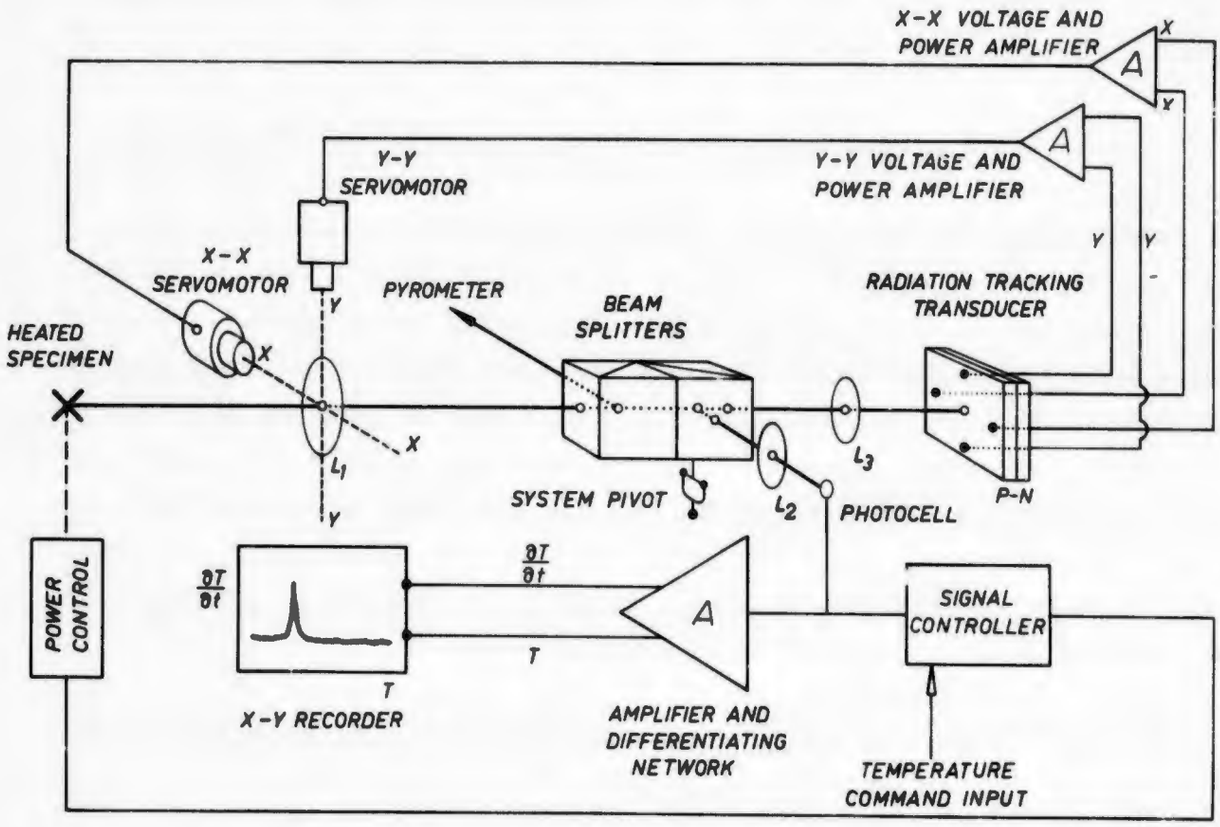

Figure 1. Principle of Operation of the Derivative Thermal Analysis Apparatus.

An enlarged image of the black body hole, after passing through a beam splitter, is focussed by the lens systems L_1 and L_2 onto a photocell, whose output is amplified and differentiated with respect to time. The time derivative of the temperature is then plotted against the amplified output by means of an X-Y recorder, or displayed on the screen of an oscilloscope. The output of the photo-diode is compared with the output of a ramp generator (temperature command input in Figure 1), thus producing an error signal, which is amplified and used to control the power delivered to the sample. For the apparatus described, controlled heating and cooling rates varying between approximately 5 and 120°C per second can be obtained.

Thermal expansion, sintering, sagging, and other effects, occurring during heating or cooling, tend to displace the radiation source relative to the detection system, causing undesirable noise in the output. To eliminate this problem, the entire radiation detection system is mounted on a X-Y tracker, each coordinate movement being independently controlled by a servomotor. Deviations from the preselected null-position are detected by focussing a separate image of the radiation source by means of a lens system L_3 onto a X-Y radiation trackingtransducer. The outputs of the tracking cell, after passing through a high gain voltage amplifier and a final power amplification stage, are used to drive the control windings of the two servomotors, thus keeping the image of the black body hole properly positioned on the photodiode throughout the experiment.

D. HIGH TEMPERATURE EQUILIBRATION AND QUENCHING STUDIES

Preliminary experiments indicated that for the majority of the high-carbon alloys the cooling rates in the tungsten vacuum furnace were too slow to regain the high temperature equilibrium states. The studies of the phase relationships prevailing at high temperature (>1400°C) were therefore carried out on alloys, which were quenched either by rapid cooling after equilibration at the desired temperature in the melting point furnace, or, more effectively, by using the quenching arrangement shown in Figure 2.

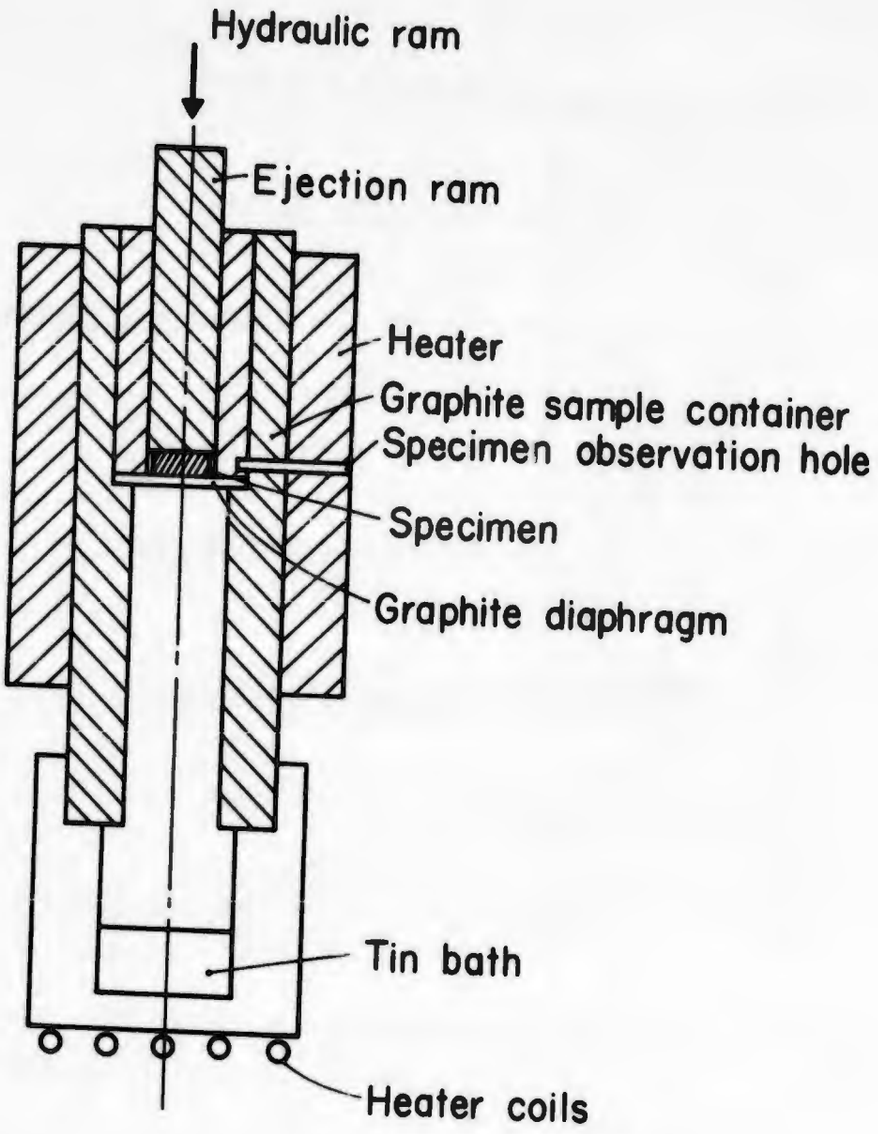

Figure 2. Experimental Quenching Arrangement.

A similar arrangement, but with the graphite diaphragm replaced by a porous graphite plug, was employed for the determination of the composition of the carbon-saturated melt (Figure 3). To achieve rapid equilibration in the latter arrangement, the molten alloy was slowly pressed through the porous graphite plug, and the carbon-saturated droplets collected and quenched in the channel protruding from the center portion of the heating element.

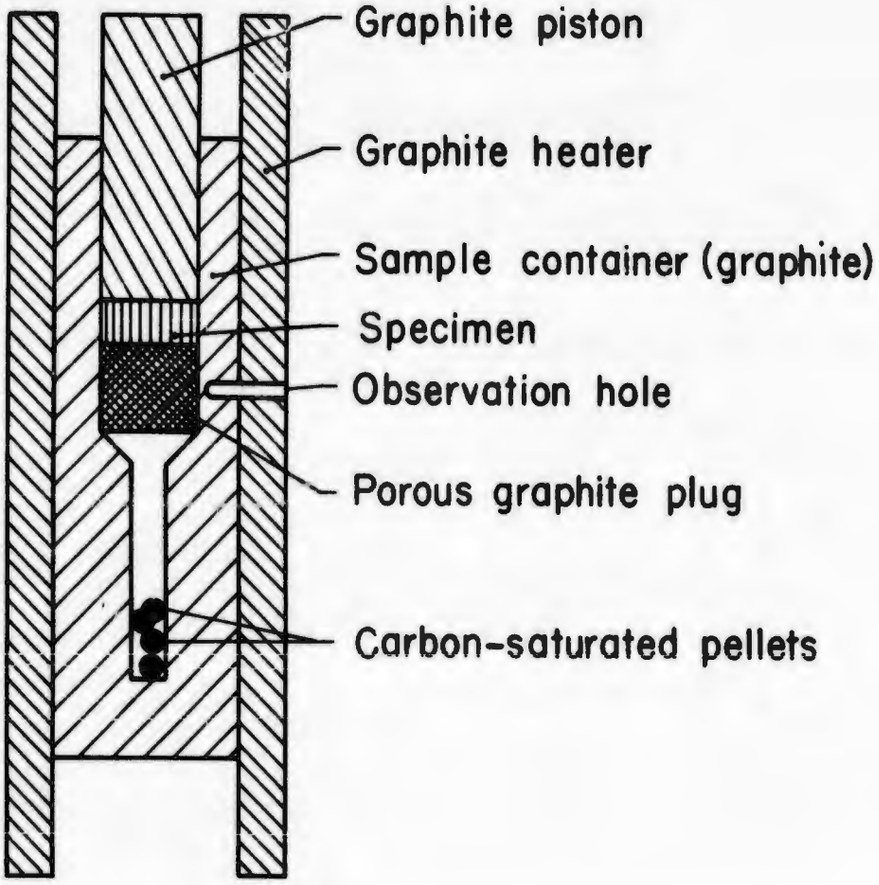

Figure 3. Experimental Arrangement for Determining the Composition of the Liquidus in Equilibrium with Graphite.

E. METALLOGRAPHIC, X-RAY, AND CHEMICAL ANALYSIS

For microscopic examinations, the specimens were mounted in a mixture of diallylphthalate and lucite-coated copper powder and pre-ground on silicon carbide papers. They were polished and etched on micro-cloth, using a slurry of Linde "B" alumina (0.05 μ) in a 5% chromic acid solution and were etched using Murakami's reagent (10 gms $K_3Fe(CN)_6$ and 10 gms KOH in 100 ml water).

Carbon was determined in the well-known manner by combustion and subsequent conductometric analysis of the gas mixture. For the determination of free carbon, the powdered alloys were dissolved in a mixture of nitric and hydrofluoric acid, the undissolved graphite flakes filtered off, and the amount of residual graphite determined by combustion. Oxygen and nitrogen were hot extracted in a gas fusion analyzer, and low level metallic impurities were determined on a semi-quantitative basis, spectrographically.

Since the crystal structures of all phases were known, only powder diffraction patterns, using CuKα radiation, were prepared from all experimental alloys.

III. RESULTS

A. PHASE EQUILIBRIA IN THE METAL-RICH PORTION OF THE SYSTEM

For molybdenum a melting point of 2619 ± 9°C was obtained from 9 measurements on samples which included cold-pressed and high vacuum-sintered, as well as electron beam melted stock. The solubility of carbon in molybdenum was not specifically investigated, but three alloys having nominal carbon contents of 0.5, 1.0, 1.5 atomic percent appeared to be all two-phased after quenching from 2000°C; the solid solubility at this temperature must therefore be lower. This finding is in agreement with earlier work[19,21,30], where the following solubility limits were reported: 0.04 to 0.07 At% C at 1650°C, 0.1 At% C at 1925°C, and a maximum of 0.15 At% at 2200°C[30]. In alloys quenched from 2200°C, however, precipitations in molybdenum became visivle, which indicates that the solubility must exceed the maximum solubilities reported previously. Based on the metallographic findings, the upper solubility limit at the eutectic temperature was placed at 1.5 atomic percent carbon.

The eutectic temperature of 2200°C was confirmed by melting point measurements (Table 3), as well as by differential thermoanalytical studies (Figure 4). The eutectic composition, located to within ± 2 atomic percent at 17 atomic percent carbon by metallographic inspection of melted alloys (Figure 5), lies about midway between the previously reported compositions.

Table 3. Melting Temperatures of Metal-Rich Molybdenum-Carbon Alloys

At% C	Number of Runs	Melting Temperatures, °C		Melting
		Incipient	Specimen Collapsed	
5.2	1	2211	2451	Heterogeneous
10.3	2	2208 ± 4	2260 ± 10	Heterogeneous
14.0	2	2204 ± 5	2205 ± 5	Fairly Sharp
18.5	2	2201 ± 4	2201 ± 4	Sharp
20.0	2	2198 ± 4	2198 ± 4	Sharp
21.6	2	2200 ± 4	2206	Slightly Heterog.
22.8	2	2206 ± 5	2221	Heterogeneous
24.1	2	2208 ± 4	2226	Heterogeneous
26.3	2	2235 ± 10	2309	Very Heterog.
27.5	2	2267 ± 8	2313	Very Heterog.

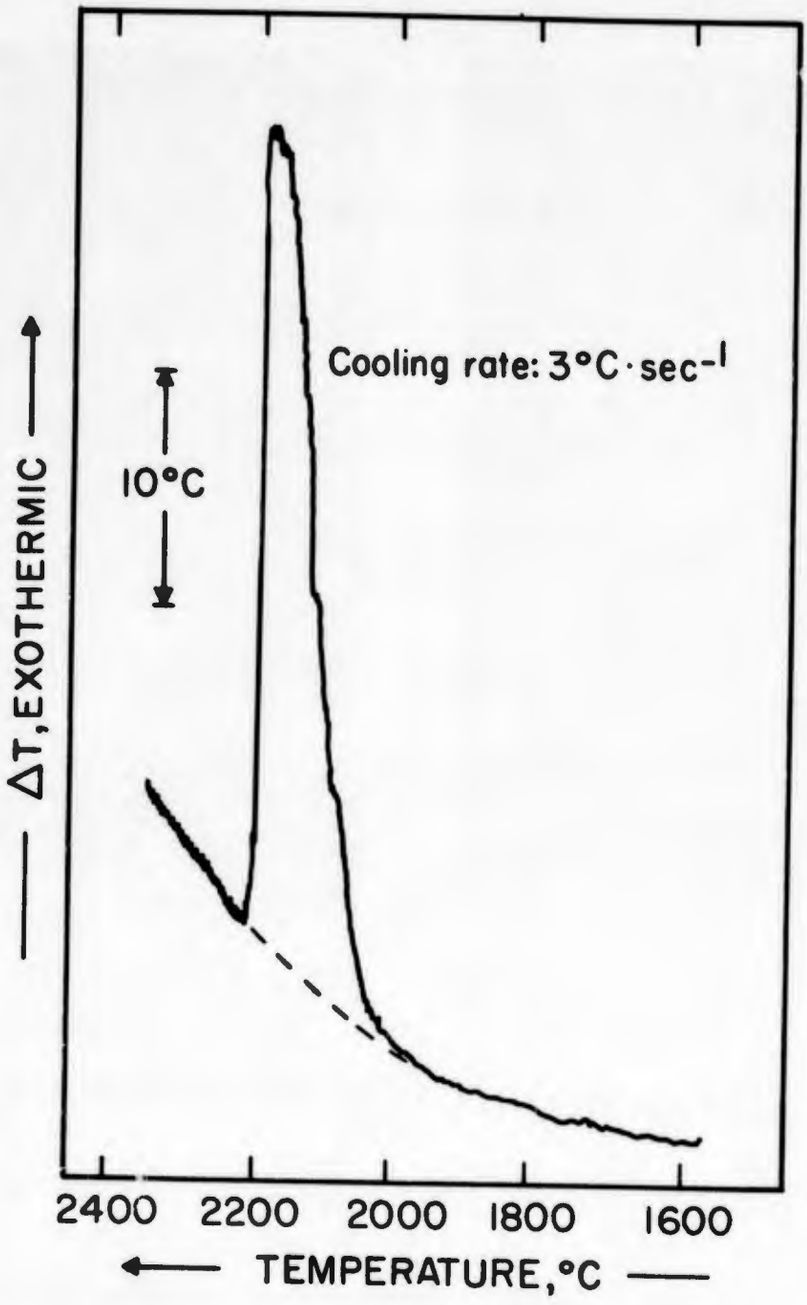

Figure 4. DTA-Thermogram (Cooling) of a Molybdenum-Carbon Alloy with 20 Atomic Percent Carbon.

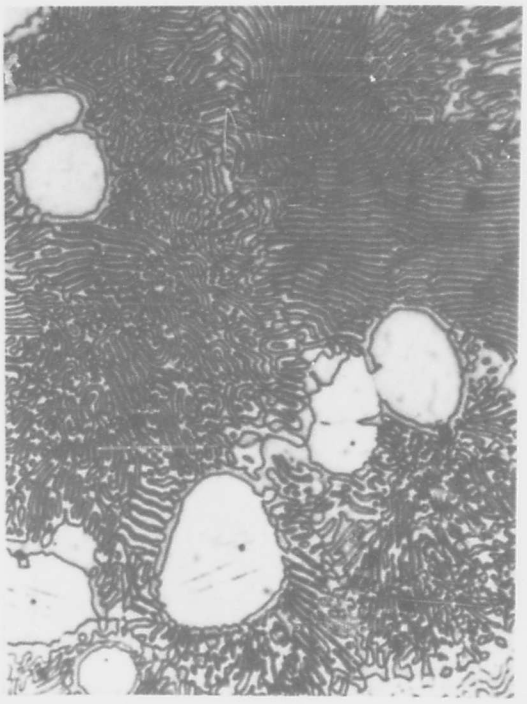

5(a) Mo-C (17 At% C) X1000 Mo + Mo_2C Eutectic

5(b) Mo-C (19 At% C) X1000 Primary Mo_2C and Eutectic

Figure 5. Micrographs of Samples in the Mo + Mo_2C Eutectic Region.

B. THE DISORDERING REACTION IN Mo_2C

DTA-runs on slightly substoichiometric alloys revealed a sharp thermal arrest at temperatures around 1400°C (Figure 6); however, the thermal behavior changes abruptly, as either stoichiometric or substoichiometric compositions are approached, or the carbon content of the alloys is further reduced. Thus, while the arrests in the alloys containing 32.5 and 32.7 atomic percent carbon are very well defined, the corresponding thermal effects in the alloy at 31.9 atomic percent carbon are smaller and occur more gradually and, furthermore, indicate the initiation of a second reaction

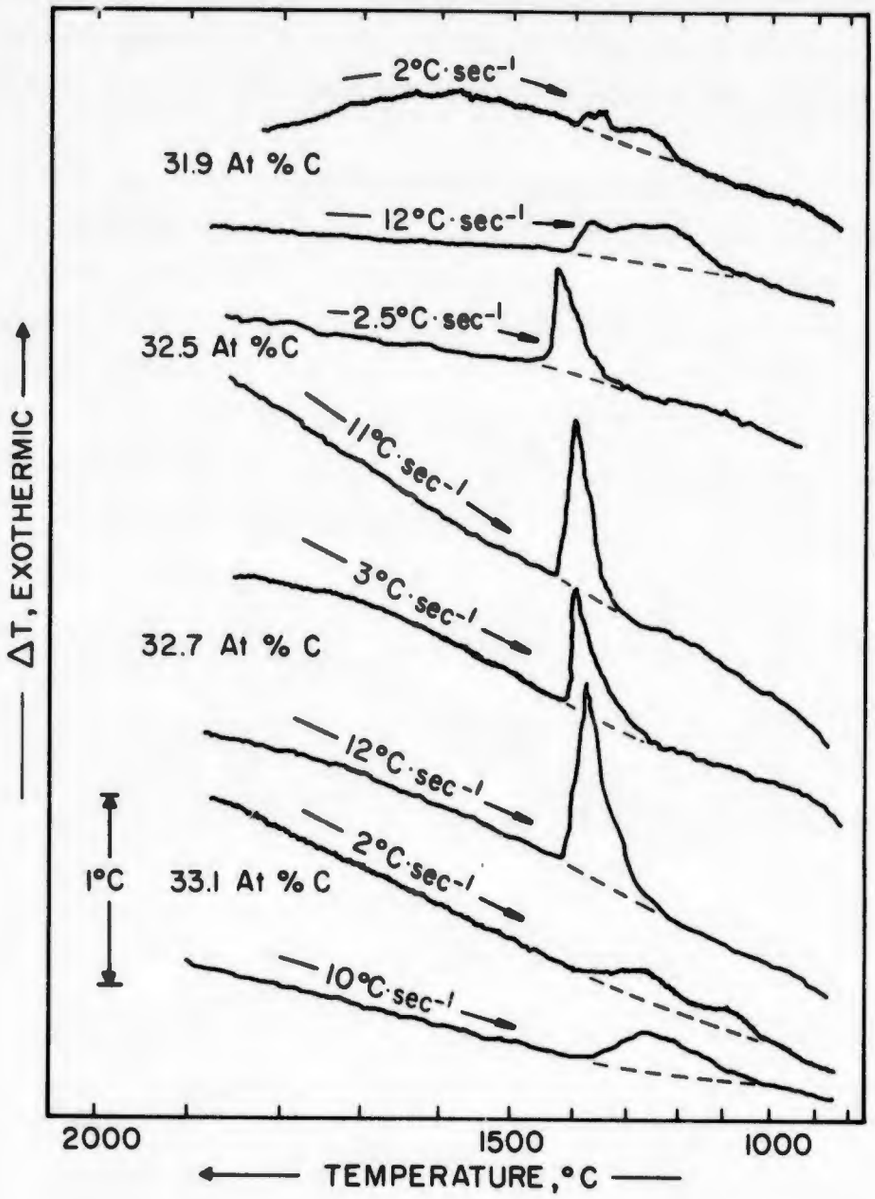

Figure 6. DTA-Thermograms (Cooling) of Mo-C Alloys Located Within the Homogeneity Range of the Mo_2C-Phase.

taking place at somewhat lower temperatures. The identical thermal arrest pattern was observed in the alloy containing 31 atomic percent carbon, although the thermal effects were still less pronounced.

Towards higher carbon contents (alloy at 33.1 At% C in Figure 6), the apparent reaction onset moves to lower temperatures, while becoming seemingly sluggish. Here again, a second thermal arrest appears at ~1200°C on the down cycle in slow speed runs, but disappears when the cooling rates exceed approximately 8°C per second. The same type of arrests, only in reverse order, appear on the heating cycle of these alloys (Figure 7).

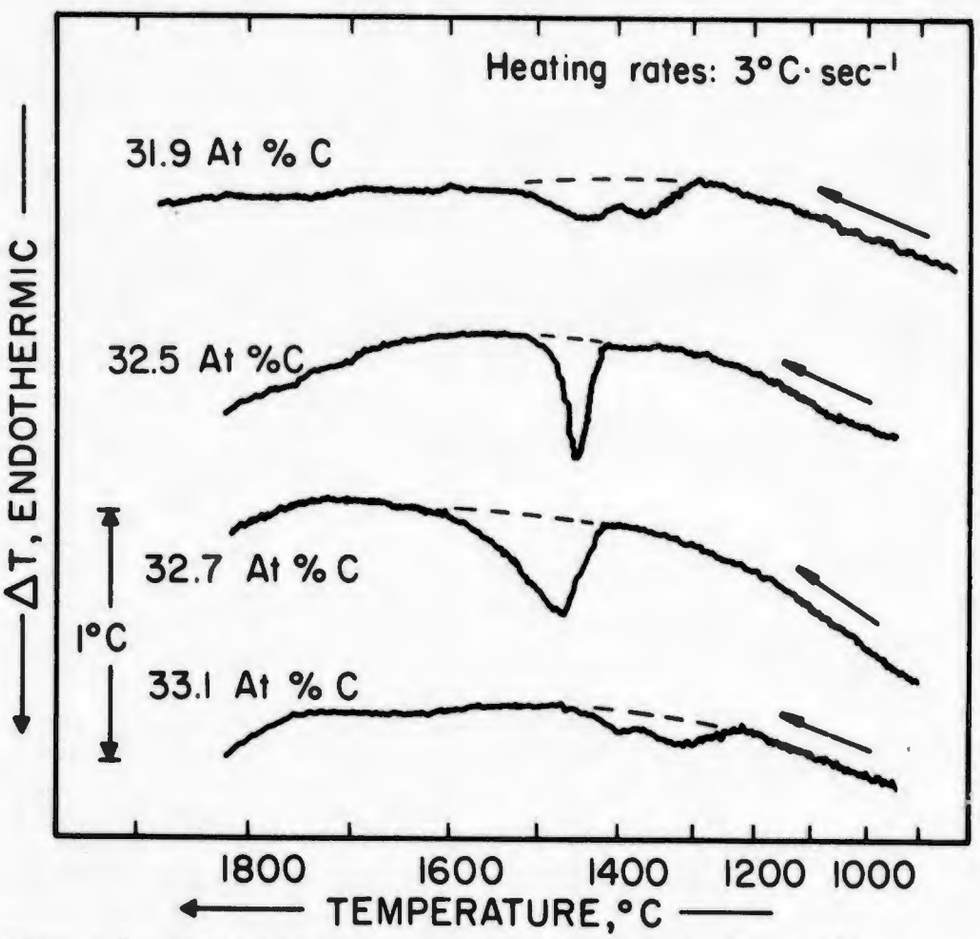

Figure 7. DTA-Thermograms (Heating) of the Same Alloys as in Figure 6.

By comparing the curves, it is especially interesting to note, that very little thermal lag and a sharp reaction onset is encountered in the alloys with 32.5 and 32.7 At% C, thus ruling out the possibility for the thermal effects to be caused by dissolution processes; in fact, the reaction within this narrow concentration range assumes all the characteristics of a first order transition, as evidenced by a thermogram taken on high sensitivity scale (Figure 8). It also appeared to be unaffected by variations in the cooling or heating speeds between approximately 0.5°C to 20°C per second. A summary of the differential thermoanalytical results on the order-disorder reaction in Mo_2C, all of which are averages from multiple runs, are summarized in the composite drawing shown in Figure 9.

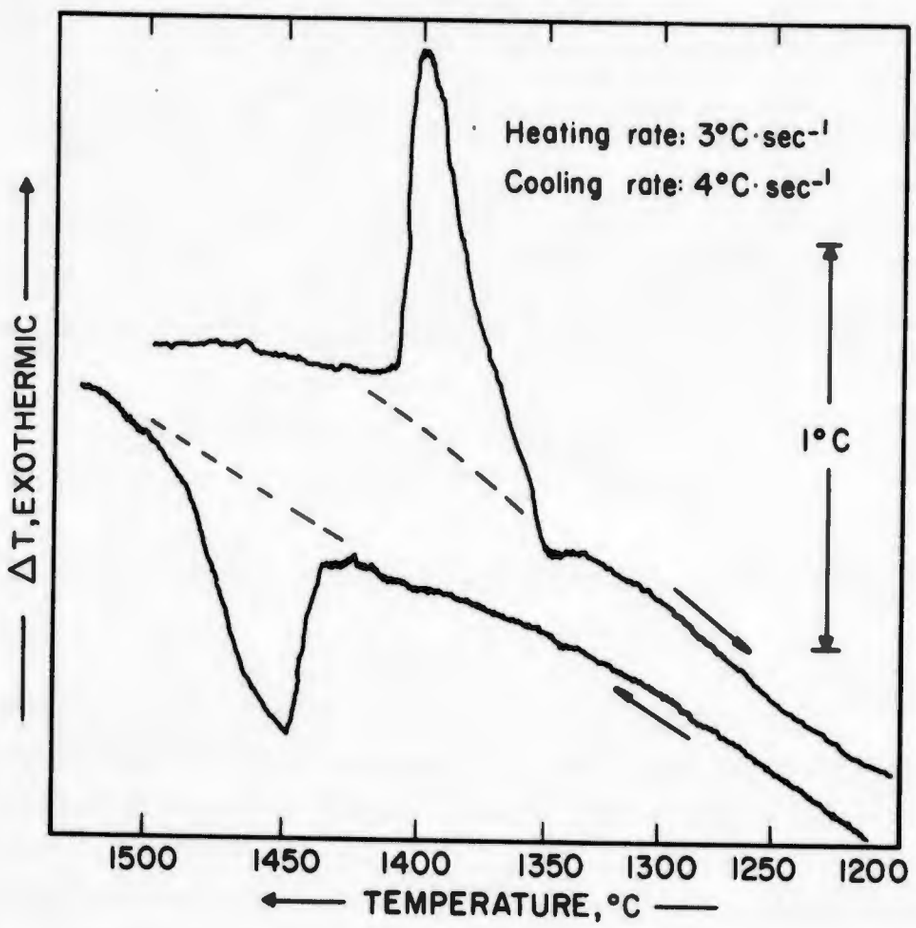

Figure 8. DTA-Thermogram of Mo_2C Containing 32.7 Atomic Percent Carbon.
(High Sensitivity Scale.)

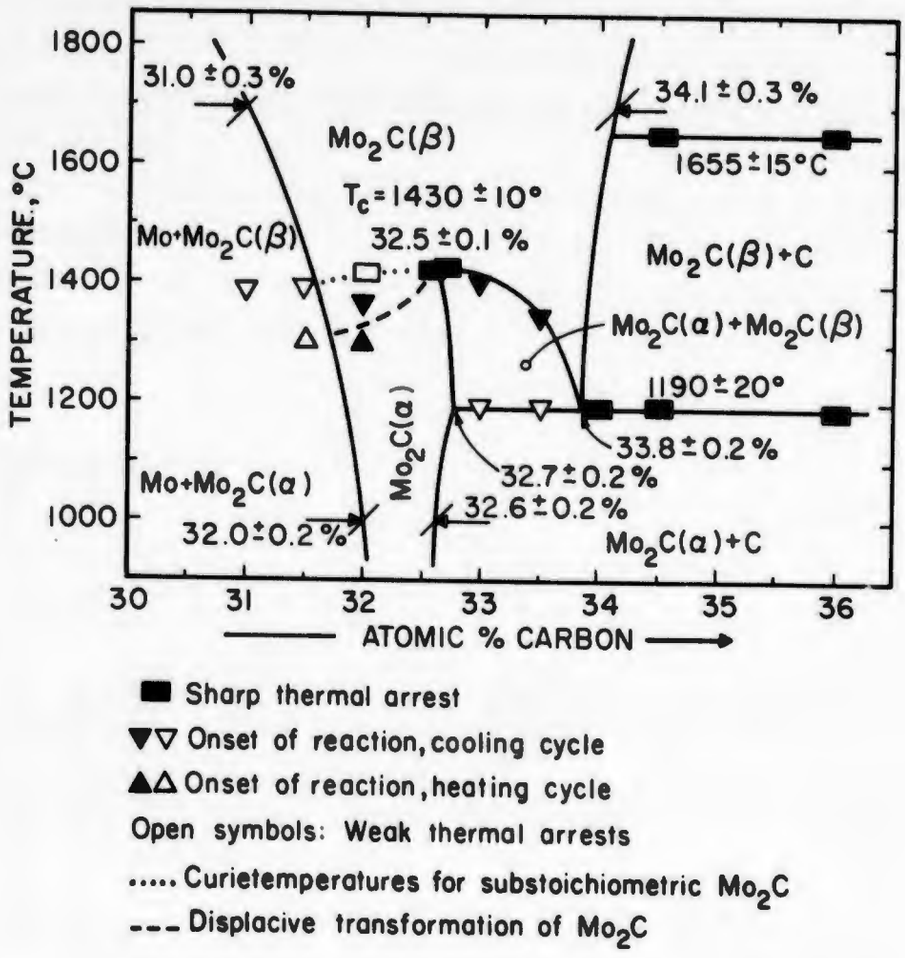

Figure 9. Summary of DTA-Results Concerning the α-β-Transition in Mo_2C.

To delineate more closely the existing phase relations in the transition region, four independent alloy series, after prehomogenization at 2000°C, were equilibrated for 1 hour at approximately 1250°, 1350°, 1470°, 1700°, and 2300°C, in the melting point furnace and quenched by shutting off the furnace power. The average cooling rates, determined by recording the calibrated output of a photodiode (Figure 1), varied somewhat with the sample configuration but were for all samples studied within the range from 90 to 120°C per second.

The temperatures of each specimen was held constant to within ± 8°C during the equilibration treatment. Each specimen was chemically analyzed after the runs and the compositions, shown in the graphical presentation of the qualitative X-ray and metallographic results in Figure 10 are believed to be accurate to ± 0.10 atomic percent. Selected specimens were reequilibrated for 20 hours at 1000°C after quenching, furnace-cooled, and also analyzed by X-ray diffraction and by microscopic examination.

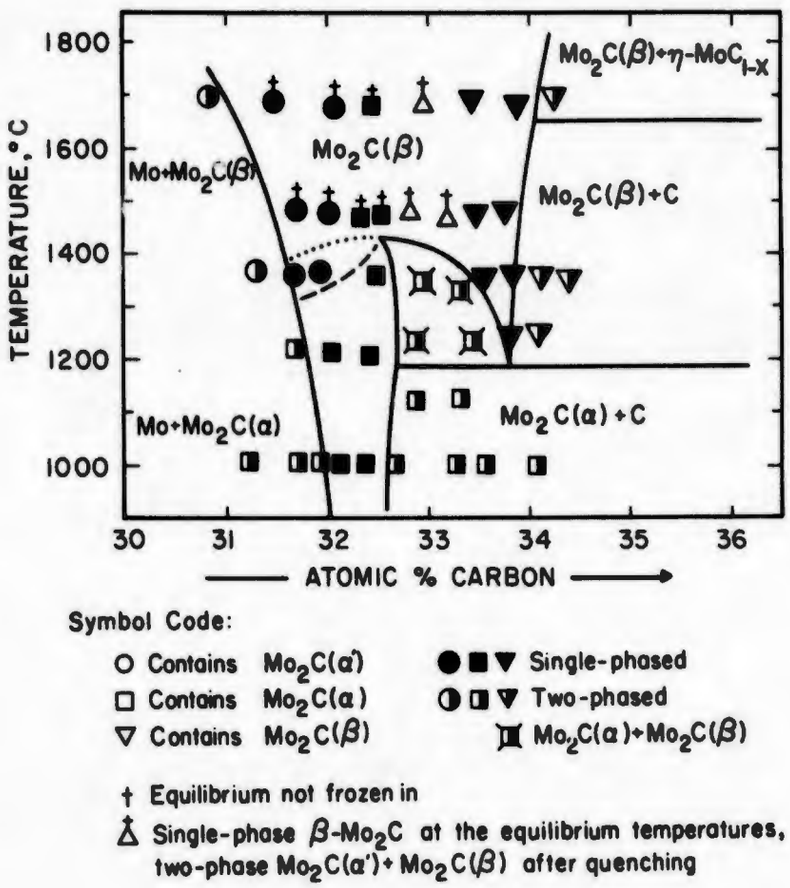

Figure 10. Order-Disorder Transition in Mo_2C: Summary of X-Ray and Metallographic Results.

The X-ray patterns of the alloy series equilibrated at 1470, 1700 and 2300°C were nearly identical, and revealed only the hexagonal close-packed metal lattice up to carbon concentrations of 32 atomic percent. Alloys in the concentration range from 32 to 32.7 atomic percent were also single-phased, but the splitting of certain reflections in the patterns indicated a slight distortion of the metal lattice. Alloys containing between 32.7 to ~33.5 atomic percent appeared to be two-phased, containing a mechanical mixture of phases with identical, or nearly identical, host lattice structures, but distinct cell dimensions (Figure 11).

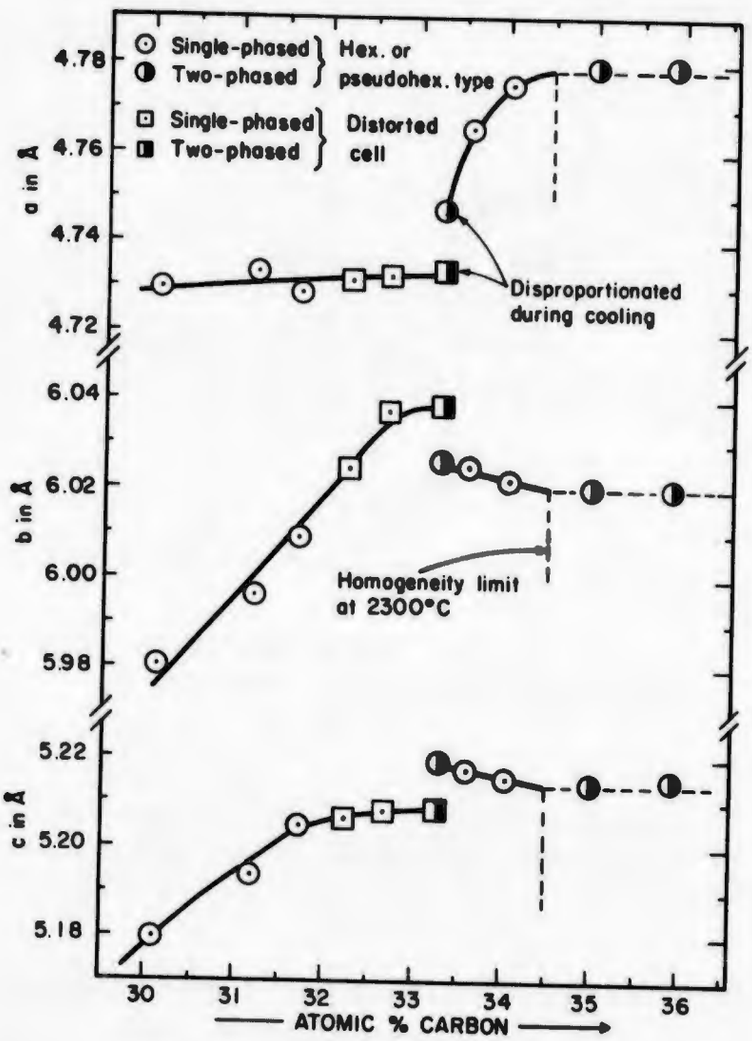

Figure 11. Lattice Parameters of Mo_2C Cooled at Approximately 100°C per Second from 2300°C. (Orthorhombic Axes)

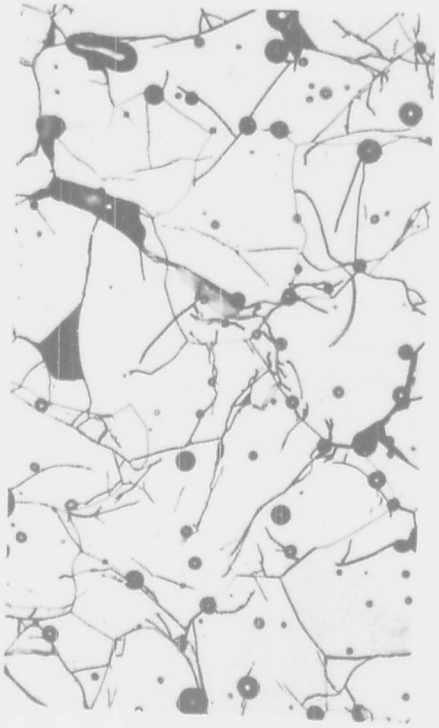

12(a) 32 At% C X250
Single Phase $Mo_2C(\alpha')$
X-ray: Mo_2C, Undistorted

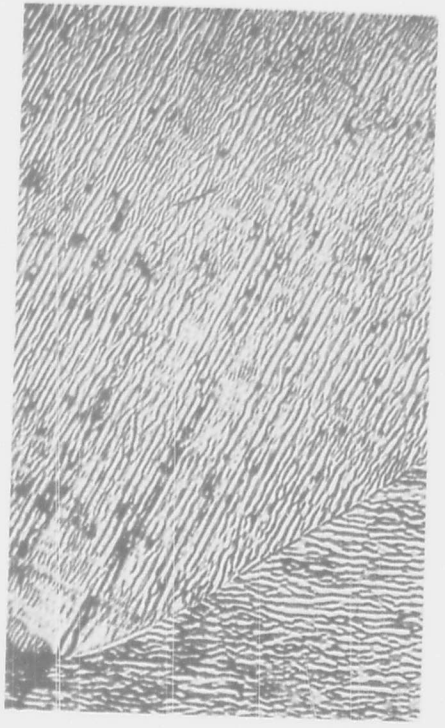

12(b) 32.9 At% C X1000
Subgrain Decomposition of $Mo_2C(\beta)$ into $Mo_2C(\alpha)$ and $Mo_2C(\beta)I$
X-ray: $Mo_2C(\alpha) + Mo_2C(\beta)$

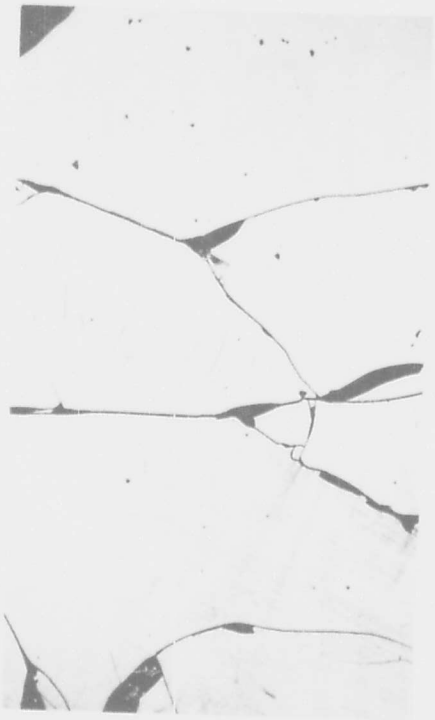

12(c) 33.8 At% C X60
Single Phase $Mo_2C(\beta)$
X-ray: $Mo_2C(\beta)$

Figure 12. Microstructures of Mo_2C-Alloys After Cooling at Approximately 100°C per Second from 1700°C.

The samples located in the composition range between 33.5 to 34 atomic percent carbon were again single-phased, and showed only the undistorted hexagonal pattern, but with significantly increased c-spacing (corresponding to the a-axis in the orthorhombic setting). The metallographic findings (Figure 12) are in essential agreement with the X-ray data (Figure 11), and furthermore indicate the presence of the phase mixture in the vicinity of the stoichiometric composition as being due to a disproportionation of an originally homogeneous phase during cooling through the critical temperature range (Figure 12-b). The occurrence of the distorted modification after rapid cooling from above 1400°C is always accompanied by the appearance of heavy slip lines within the Mo_2C-grains (Figure 13).

Figure 13. Slip Lines in Mo_2C (32.5 At% C). X475
Alloy Cooled at ~100°C per Second from 1700°C.

(Vertically Illuminated for Improved Phase Contrast.)

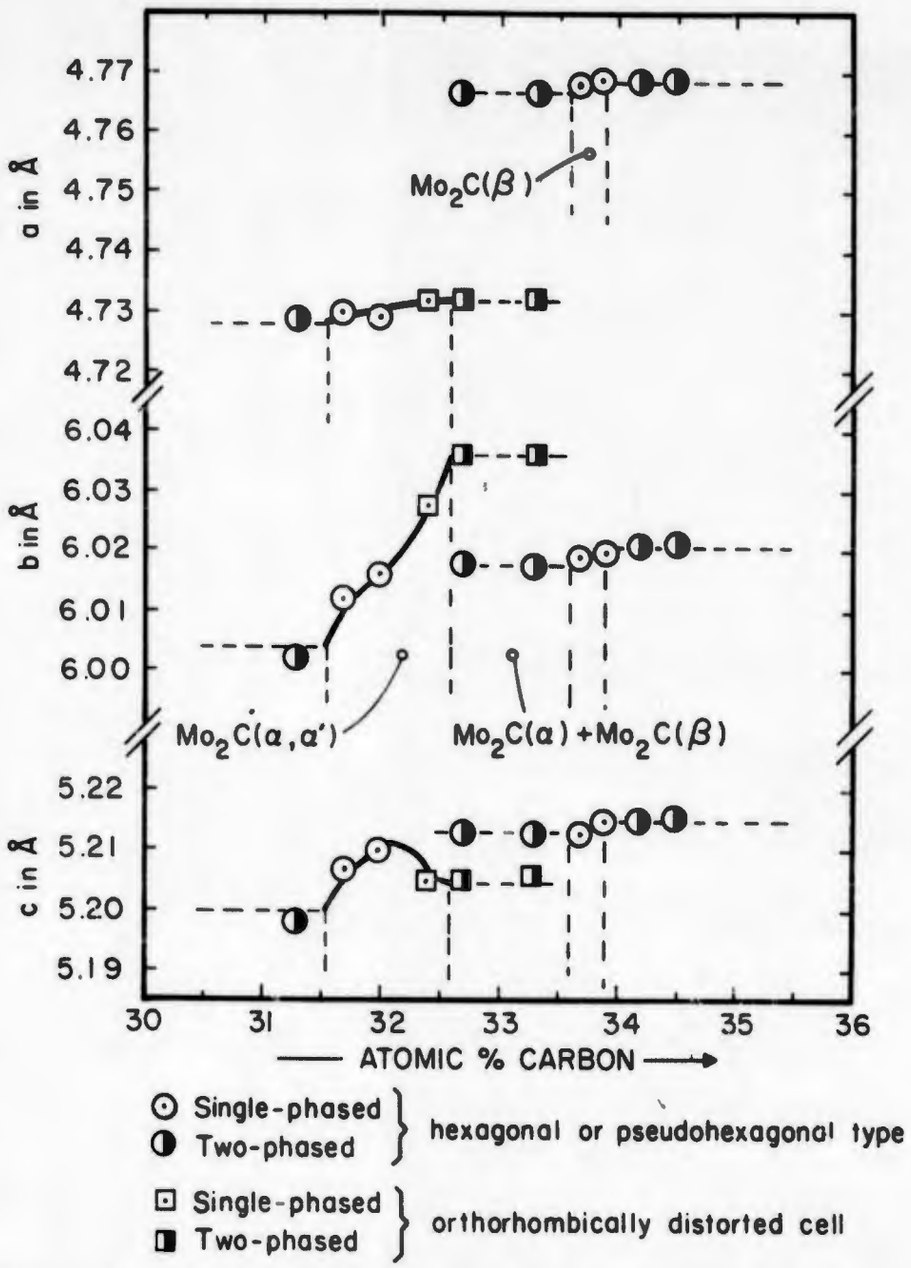

Figure 14. Lattice Parameters of Mo_2C, Quenched After Equilibration at 1350°C.

Essentially the same findings were obtained in the alloy series equilibrated at 1350°C, although the two-phase gap between the two modification appears somewhat larger; the displacive transformation leading to the distortion of the hexagonal or pseudohexagonal cell is such that one axis becomes elongated whereas the other one appears compressed with respect to the ideal dimensions of the hexagonal lattice (Figure 14).

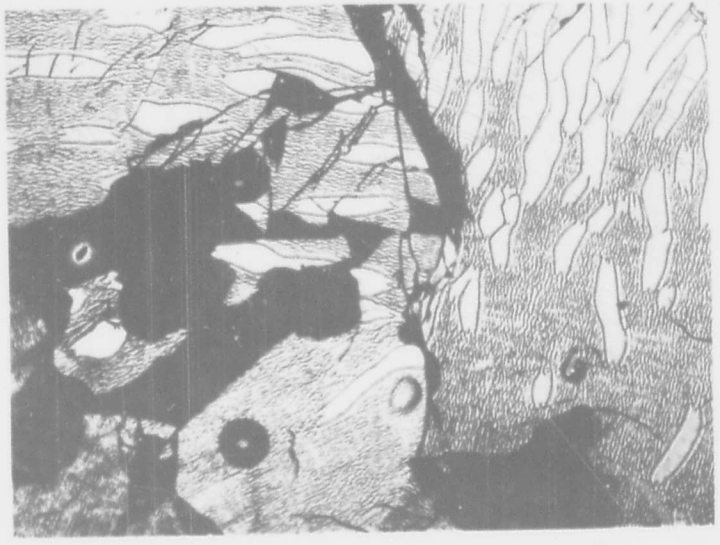

15(a) X350

Note Varying Orientation in the Different Grains

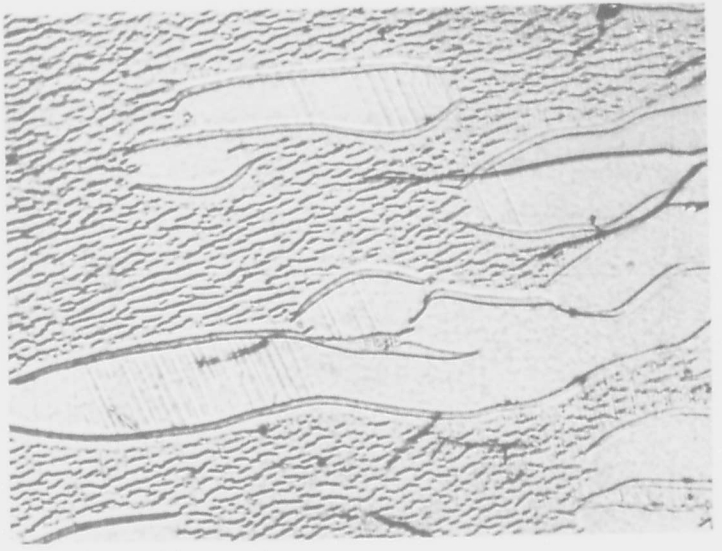

15(b) X1000

Growth Twins Within the $Mo_2C(\alpha)$-Grains

Figure 15. Collective Recrystallization of the $Mo_2C(\alpha)$ + Mo $C(\beta)$ Decomposition Structure at 1350°C. Alloy: Mo-C (32.8 At% C), Homogenized at 2000°C, Reequilibrated for 30 Minutes at 1350°C, and Quenched.

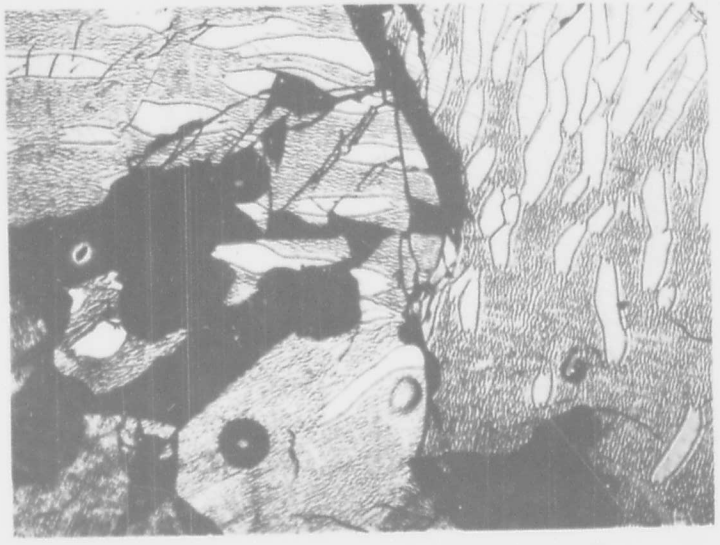

15(a) X350

Note Varying Orientation in the Different Grains

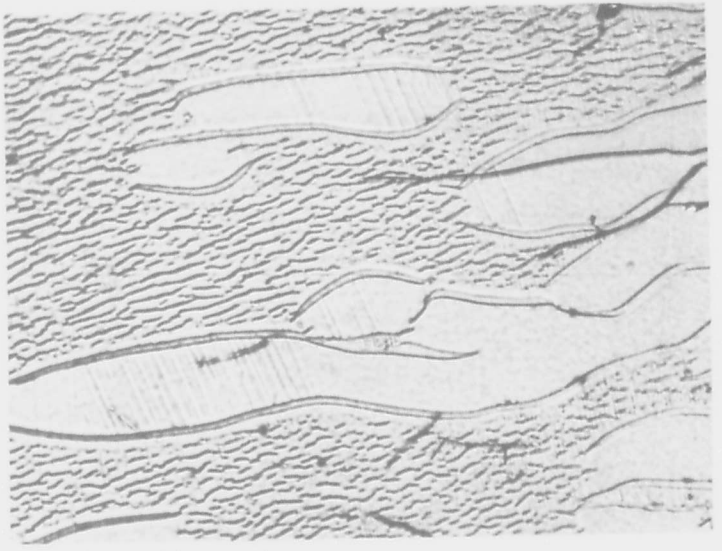

15(b) X1000

Growth Twins Within the $Mo_2C(\alpha)$-Grains

Figure 15. Collective Recrystallization of the $Mo_2C(\alpha)$ + Mo $C(\beta)$ Decomposition Structure at 1350°C. Alloy: Mo-C (32.8 At% C), Homogenized at 2000°C, Reequilibrated for 30 Minutes at 1350°C, and Quenched.

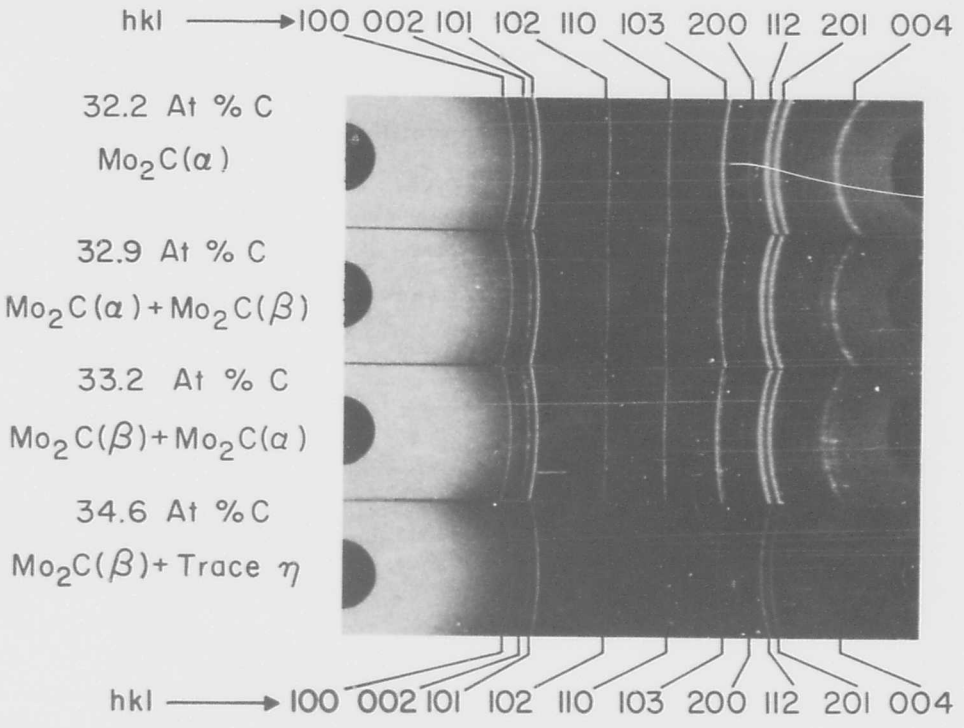

Figure 17. Coexistence of $Mo_2C(\alpha)$ and $Mo_2C(\beta)$ in the Alloy Series Quenched after Equilibration at 1350°C. (Hexagonal Indices)

Proof for the existence of Mo_2C as a single, homogeneous phase at temperatures above 1430°C was finally established by equilibration of a sample series at 1700°C followed by rapid quenching in tin. The X-ray patterns of this alloy series showed only the undistorted modification and a continuous, although unexpected, variation of the cell-dimension with the carbon content (Figure 18). The metallographic examination also revealed only a single phase.

The eutectoid (pseudomonotectoid) decomposition of the $Mo_2C(\beta)$-phase, indicated by differential thermal analysis to occur in the

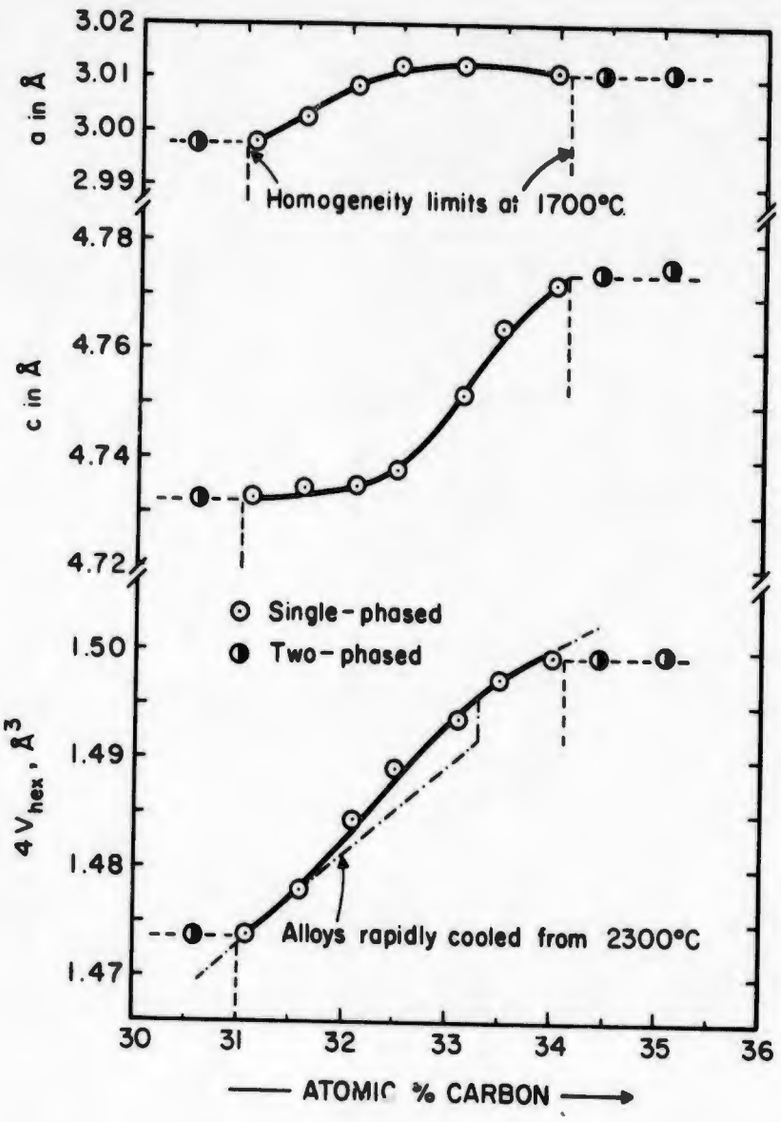

Figure 18. Lattice Parameters and Unit Cell Volume of Mo_2C in Tin-Quenched (1700°C) Alloys. (Hexagonal Axes)

vicinity of 1200°C, (Figure 6) was studied and confirmed by X-ray and metallographic, as well as by chemical analytical means on specimens which were equilibrated at temperatures slightly above and below the isothermal reaction line, and then quenched. The reaction (Figure 19) is a nucleation and growth process, and proceeds with comparatively low speed in alloys with less than 33.8 atomic percent carbon; the observed higher reaction rates in hypereutectoid compositions leads one to suspect that nucleation of the graphite phase might be the rate-determining step.

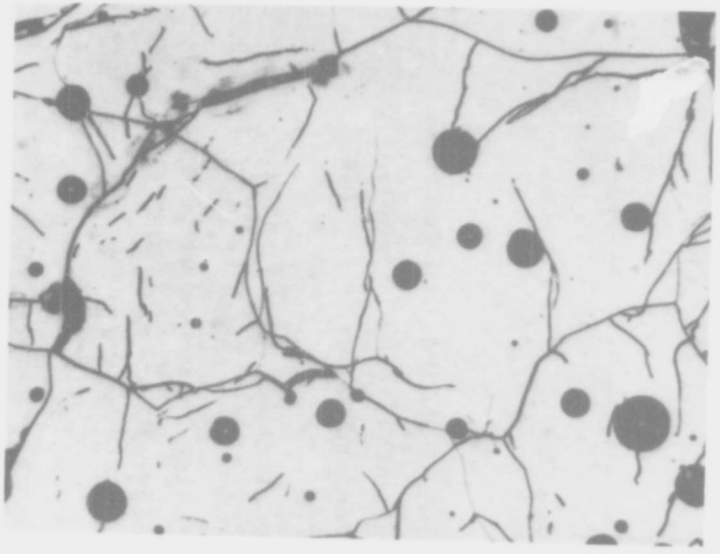

19(a) 1230°C X1000

X-ray: $Mo_2C(\beta)$

C_{bound} = 33.8 At% C

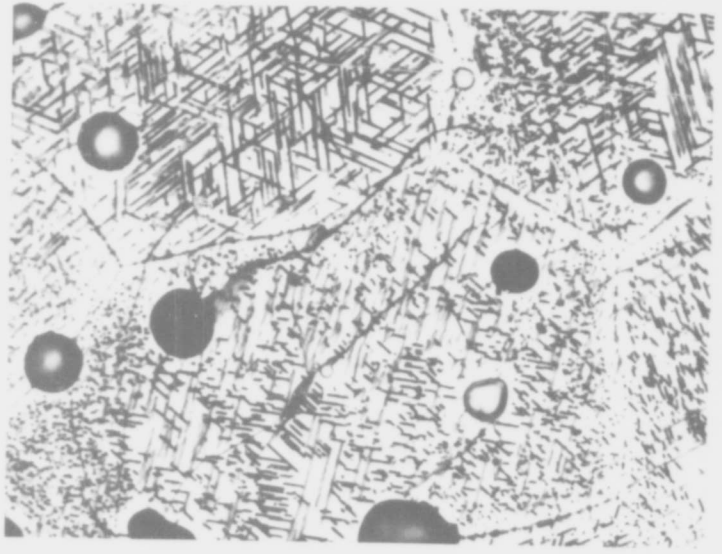

19(b) 1230°C + 2 hrs at 1160°C X1000

X-ray: $Mo_2C(\alpha)$ + Graphite

C_{bound} = 32.7 At% C

Figure 19. Eutectoid (Pseudomonotectoid) Decomposition of Hyperstoichiometric $Mo_2C(\beta)$ at Temperatures Below 1200°C.

Phase homogeneity at 1000°C exists between 32.0 and 32.6 atomic percent carbon; the only modification present at this temperature is the distorted ordered form of Mo_2C, having lattice parameters of a=4.731 Å, b=6.027 Å, c=5.199 Å, at the low carbon end, and a=4.733 Å, b=6.042 Å, c=5.202 Å in alloys containing excess graphite.

Independent experimental evidence for the reactions occurring in Mo_2C within a very limited composition interval was also gained through diffusion experiments performed at 1100°C, 2200°C, and 2000°C. The base alloys, consisting of molybdenum and of Mo_2C (32 At% C), were prepared by hot-pressing in graphite dies. After hot-pressing, the excess graphite from both ends of the cylindrical specimens was cut off, and interdiffusion between the sample core and the graphite shell allowed to take place, while heated under high purity helium.

In the experiment series conducted at 1000°C, only one interface layer, identified as $Mo_2C(\alpha)$ by X-ray diffraction, had formed between graphite and molybdenum. In the high temperature experiments, three distinct carbido phases, corresponding to Mo_2C, η-MoC_{1-x}, and α-MoC_{1-x}, are discernible (Figure 20). The zone adjacent to the core containing excess molybdenum shows the characteristic unidirectional molybdenum precipitations in substoichiometric (<30 At% C) dimolybdenum carbide. The veining-type substructure adjacent to the single phase zone consists of disproportionated β-phase. Although the interface appears, at a first glance, to be relatively sharp, a closer examination reveals (Figure 21) that no true phase boundary does exist.

With increasing carbon contents, the veining-type decomposition structure gradually disappears and is replaced by a single-phase region at the eutectoid composition, where the comparatively slow reaction rates have retained the $Mo_2C(\beta)$-phase.

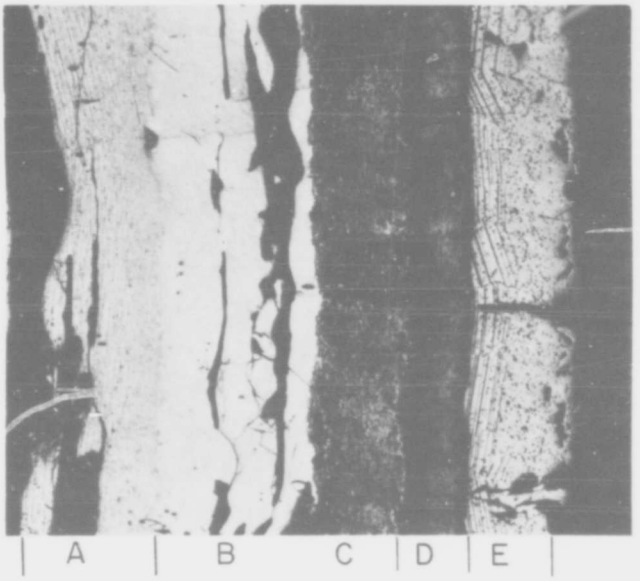

X100

Figure 20. Molybdenum + Graphite Diffusion Couple (14 Minutes at 2300°C, Cooled at 14°C per Second).

A..... Mo_2C with Molybdenum Precipitations
B..... $Mo_2C(\alpha, \alpha')$
C..... $Mo_2C(\alpha) + Mo_2C(\beta)$, Disproportionated During Cooling
D..... $Mo_2C(\beta)$, with Precipitations of η-MoC_{1-x}
E..... η-MoC_{1-x} + α-MoC_{1-x}

The microstructure of the compositions lying between that of the eutectoid and the interface Mo_2C——η-MoC_{1-x} is characterized by heavy, unidirectional precipitation on η-MoC_{1-x} from the hyperstoichiometric dimolybdenum carbide formed during cooling (Figures 22 and 23). The sequence of phases present in the various diffusion zones was also confirmed by X-ray diffraction analysis of the mechanically separated reaction layers.

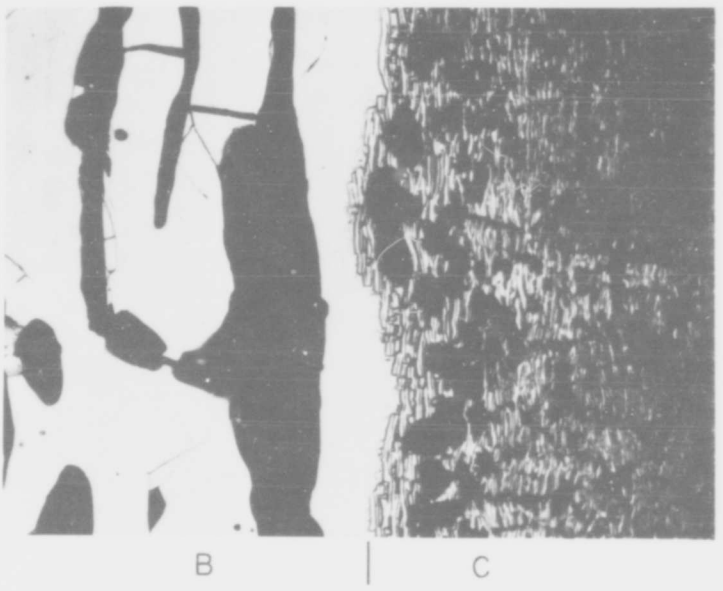

Figure 21. Zone B-C of the Diffusion Couple Shown in Figure 20. X400

Gaps (Black) are Due to Differential Thermal Expansion During Cooling.

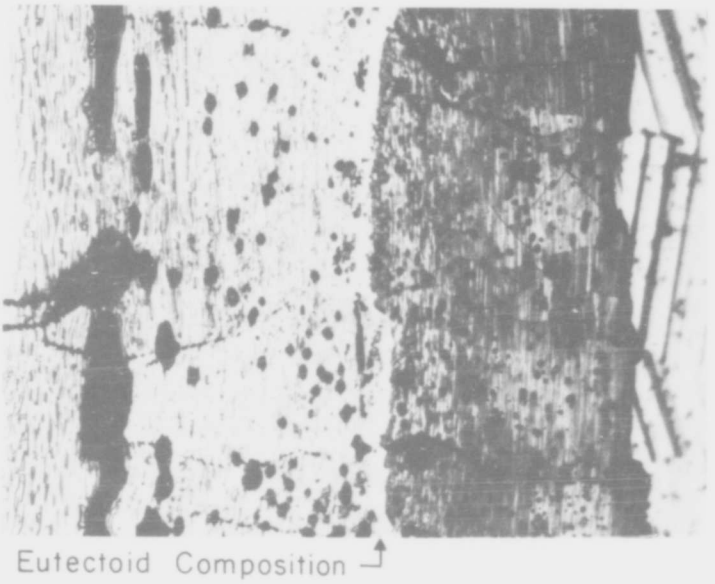

Figure 22. Zone C and D of the Diffusion Couple Shown in Figure 20. X400

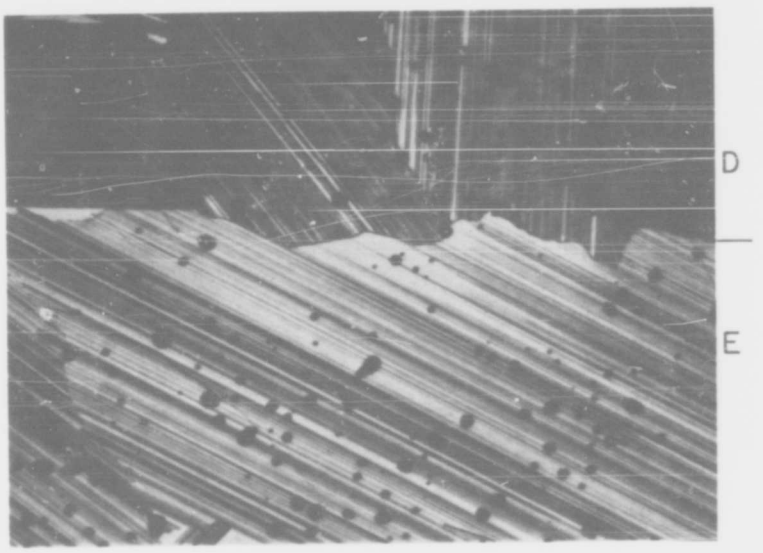

X600

Figure 23. Zone D-E from the Sample Shown in Figure 20.

Unidirectional Precipitation of η-MoC_{1-x} from Hyperstoichiometric $Mo_2C(\beta)$(D), and Partially Decomposed η-MoC_{1-x}(E).

C. MELTING AND HIGH TEMPERATURE HOMOGENEITY RANGE OF Mo_2C

Towards higher temperatures, the width of the homogeneous range of the Mo_2C-phase increases. The phase extends from 26 to 34.4 At% C at the Mo + Mo_2C eutectic temperature, and to approximately 36 At% C at 2510°C, the temperature of the reaction isotherm $Mo_2C(\beta)$ + η-MoC_{1-x}. Precipitation of molybdenum from alloys containing less than 30 atomic percent carbon occurs very rapidly and could not be prevented in our experiments, nevertheless, the high temperature phase boundaries could be delineated fairly accurately by the appearance of the microstructures following quenching (Figure 24). Precipitation of η-MoC_{1-x} from the hyperstoichiometric (> 34.5 At% C) carbide also appeared to be fast, and alloy compositions beyond approximately 34.7 At% C were not retained single-phased.

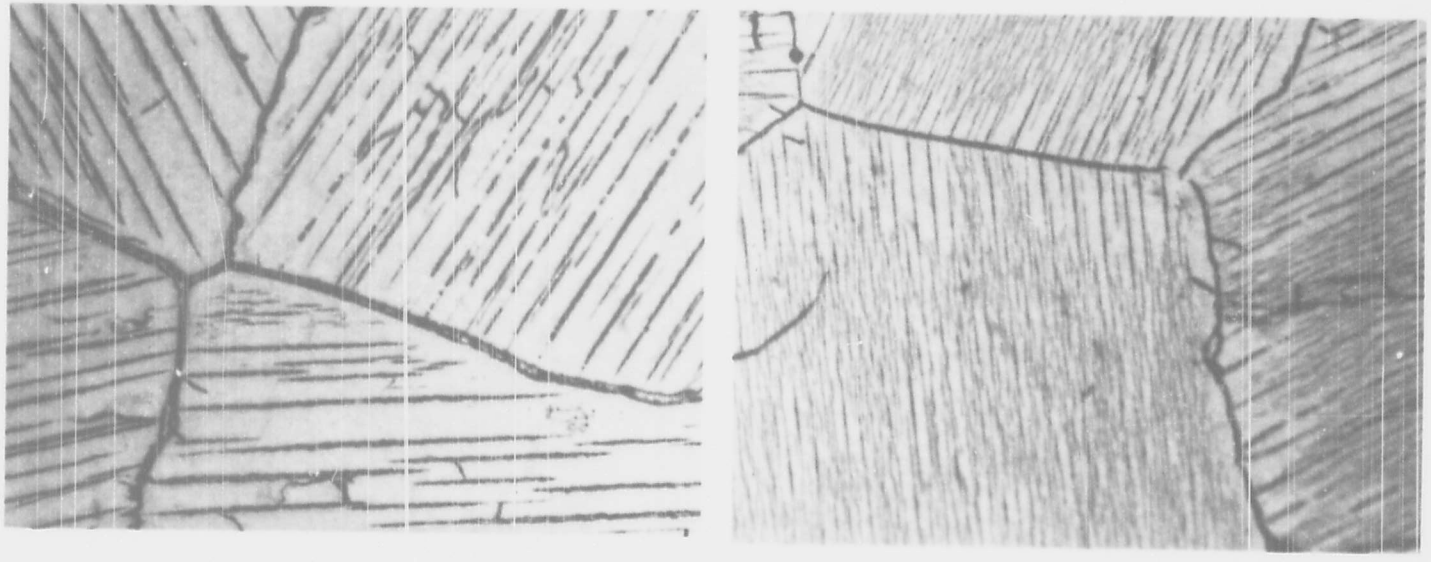

24(a) 25.5 At% C X1000 24(b) 26 At% C X1000

Figure 24. Low Carbon Boundary of Mo_2C at the Mo + Mo_2C Eutectic Temperature. (Alloys Quenched from 2210°C).

(a) Mo_2C with Unidirectional Molybdenum Precipitations and Small Amounts of Excess Molybdenum at the Grain Boundaries.

(b) Single Phase Mo_2C at the Equilibrium Temperature.

The solidus temperatures of the Mo_2C-phase were determined on three independent alloy series, whose compositions were ascertained to ± 0.2 At% C by chemical analyses performed after the runs. The average reproducibility limits in the temperature measurements were better than ± 10°C. Although the measured data do indicate a melting anomaly in the vicinity of 32.5 At% C (Figure 25) the small temperature differences involved probably do not justify assuming the existence of a melting point minimum at this composition.

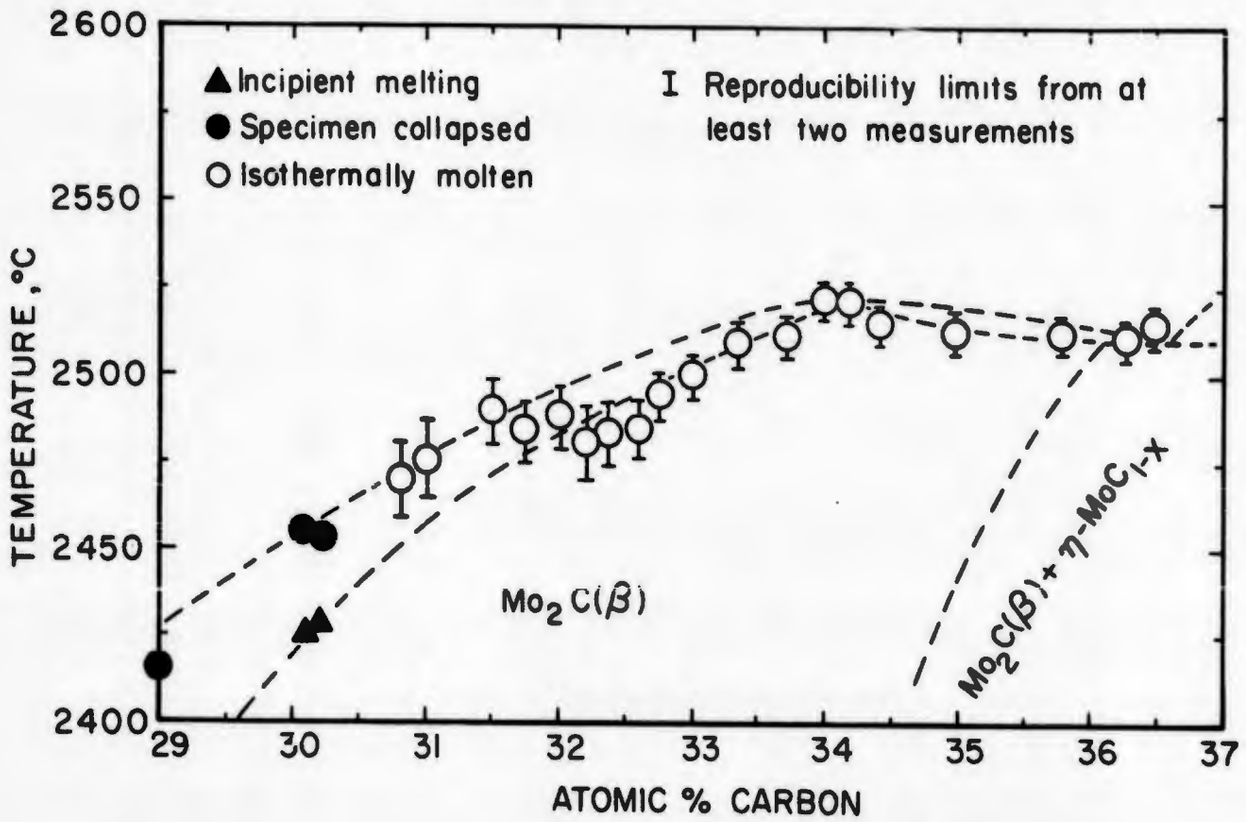

Figure 25. Experimentally Observed Melting Temperatures for Mo_2C Alloys.

D. THE HIGH TEMPERATURE PHASES η-MoC_{1-x} AND α-MoC_{1-x} PHASE EQUILIBRIA IN THE CARBON-RICH PORTION OF THE SYSTEM.

Two closely spaced melting point maxima, one at ~ 39 At% C and 2550°C, and the other occurring at 42 At% C and 2600°C (Figure 26), were identified as being due to congruent melting of the η-MoC_{1-x} and the α-MoC_{1-x} phase, respectively. The formation of a eutectic at ~2580°C is further indicated by the slight drop in the melting temperatures in the alloys located beyond the congruently melting composition of α-MoC_{1-x}.

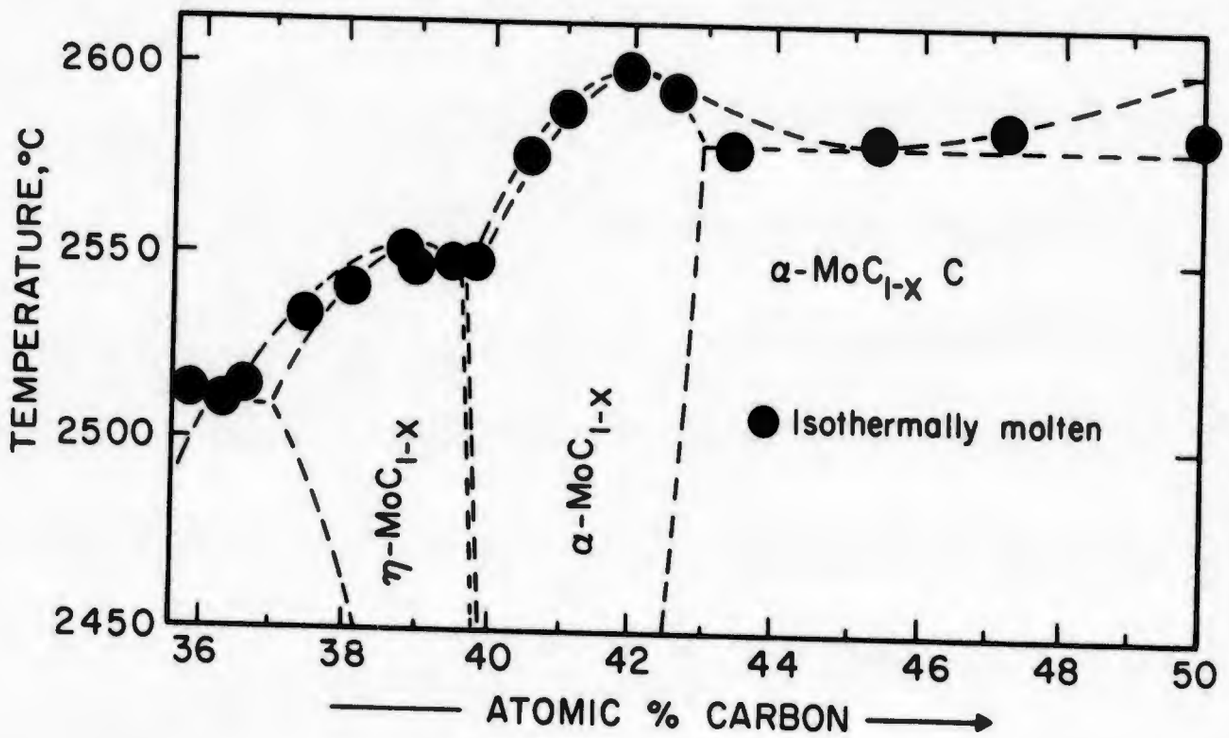

Figure 26. Melting in Carbon-Rich Alloys. (Average Reproducibility Limits ± 5°C, ± 0.3 At% C).

Note: Due to the small temperature intervals between the solidus and liquidus curves, the specimens appeared to melt isothermally.

The homogeneous range of η-MoC_{1-x} at temperatures up to 2000°C was found to be small (Figure 27), and extends to larger defect compositions only at temperatures approaching melting. However, due to the extremely rapid rates of disproportionation, it proved to be impossible to retain alloys with less than 38 At% C as a single phase.

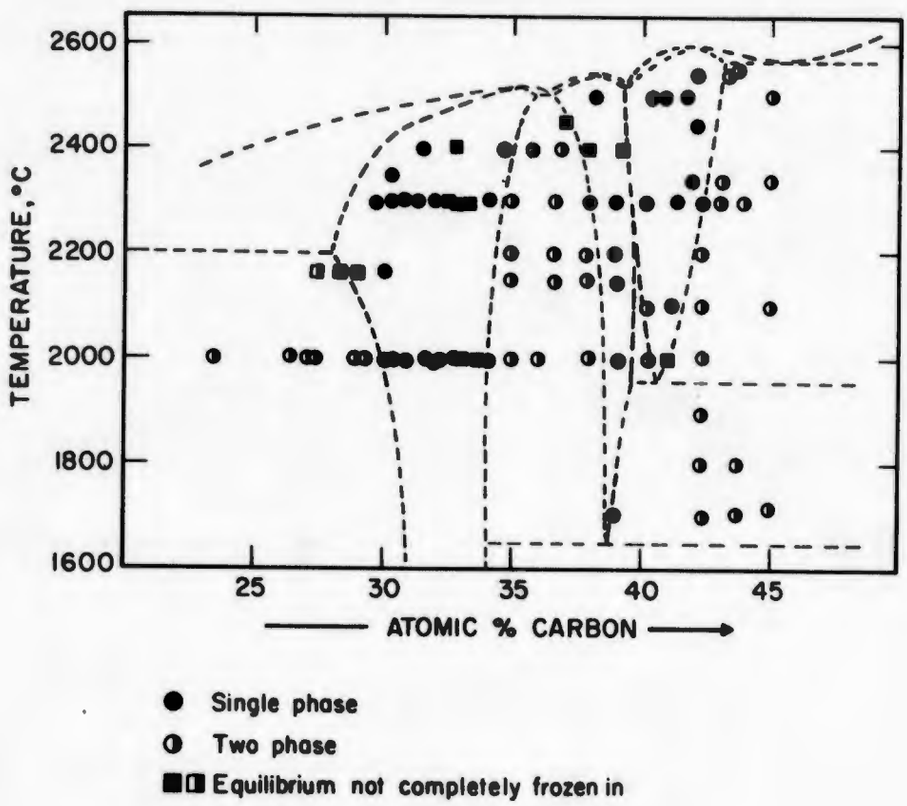

Figure 27. Compositions and Equilibration Temperatures of Experimental Alloys, and Qualitative Phase Evaluation on the Quenched Alloys.

In concurrence with the results of the quenching studies, only two reaction isotherms, one associated with the previously discussed eutectoid decomposition of the disordered modification of Mo_2C, and the other corresponding to the eutectoid temperature of the η-MoC_{1-x} phase were revealed in DTA runs on alloys with carbon contents between 34.5 to 39 atomic percent (Figure 28). It also appeared from these measurements, that both phases are stable up to their respective melting temperatures, i.e., η-MoC_{1-x}, in spite of its structural similarity to α-MoC_{1-x}, does not transform into the cubic modification at high temperatures as previously suggested[10, 14].

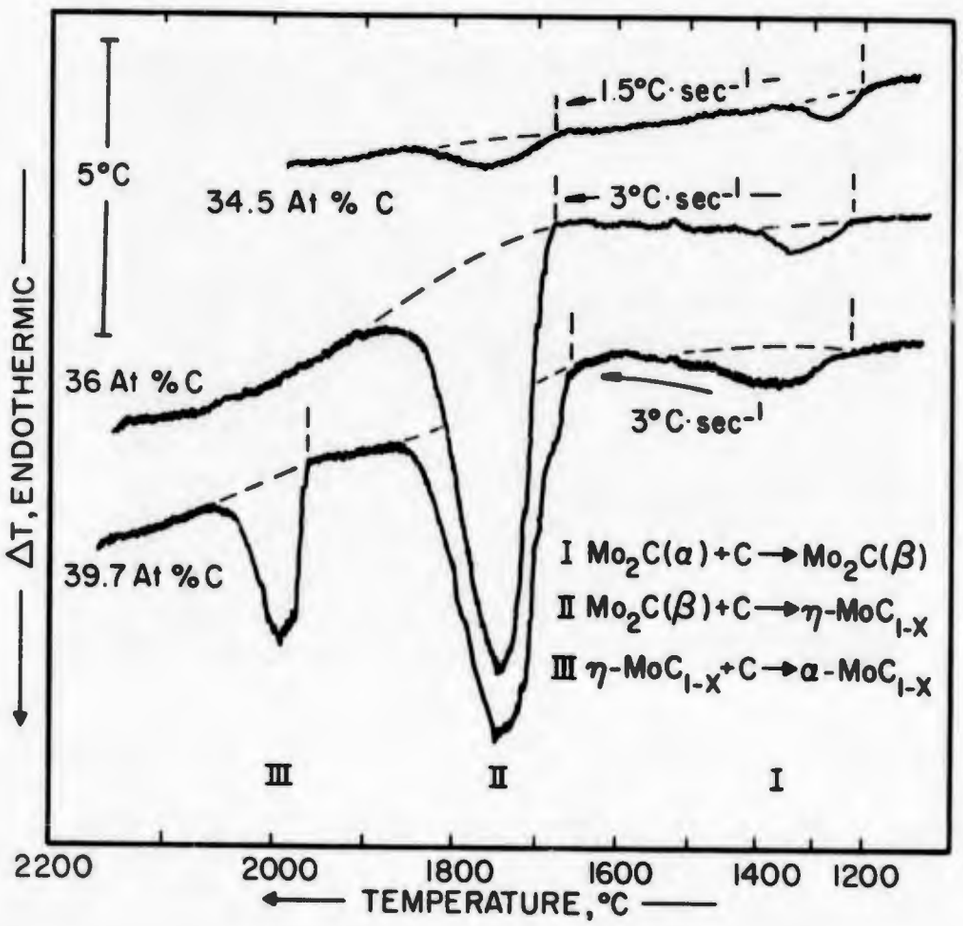

Figure 28. DTA-Evidence for the High Temperature Phase Reactions in Molybdenum-Carbon Alloys with Carbon Contents Between 34.5 and 39.7 Atomic Percent.

The eutectoid composition was located at 39 $\pm$ 0.5 At% C by chemical analysis as well as by metallographic inspection of tin-quenched alloys (Table 4). In conjunction with the eutectoid disproportionation of the η-MoC_{1-x} phase it may be worth noting that although the initiation of the decomposition reaction (Figure 29) appears to be a comparatively rapid process, fairly long annealing times at subeutectoid temperatures are necessary in order to complete the reaction, i.e. to decompose the η-MoC_{1-x} phase completely. The presence of small amounts of η-phase in the lower temperature (> 1600°C) annealing and quenching experiments presented in Table 4 have therefore, to be interpreted as rising from kinetic effects.

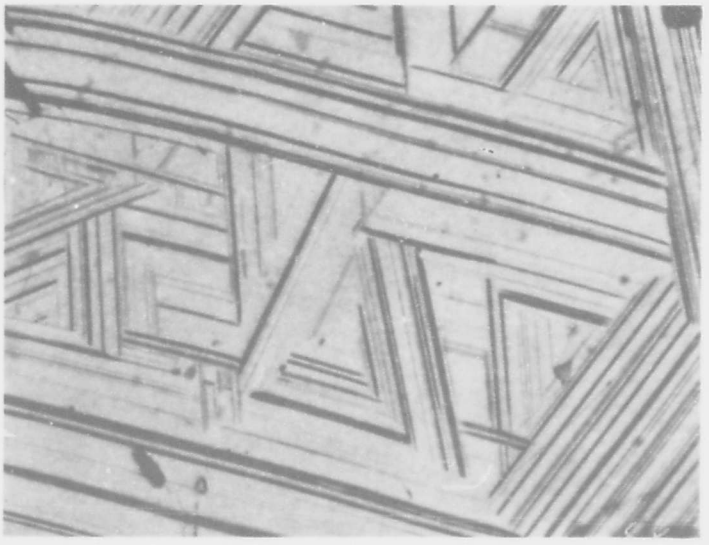

X1000

Figure 29. Mo-C (38 At% C), Cooled at 20°C per Second from 2500°C.

Incipient Decomposition of η-MoC_{1-x} into Mo_2C and Graphite.

Table 4. Formation of η-MoC_{1-x} from β-Mo_2C and Graphite: Analytical and X-ray Results on Quenched Specimens.

No	Quenching or Annealing Conditions	Analyt. Determ. Composition, Atomic % Carbon Total	Bound	Phases Present (X-ray)	Lattice Parameters	Remarks
1	30 hrs /1500°C	42.5	33.6	α-Mo_2C + β-Mo_2C + graphite + traces η-MoC_{1-x}	n.d.	η-MoC_{1-x} not completely decomposed
2	25 min/1600° ↓	45.0	~34.0	β-Mo_2C + traces η-MoC_{1-x}	n.d.	η-MoC_{1-x} not completely decomposed
3	8 min/1700° ↓	39.0	39.0	η-MoC_{1-x}	a=3.010Å, c=14.64Å } η-MoC_{1-x}	
4	10 min/1700° ↓	42.5	38.9	η-MoC_{1-x} + C	n.d.	
5	10 min /1720° ↓	45.0	38.3	η-MoC_{1-x} + C	n.d.	
6	10 min/1800° ↓	42.4	39.5	η-MoC_{1-x} + C	a=3.011Å, c=14.64Å } η-MoC_{1-c}	
7**	10 min /1700° + 25 min 1500° ↓	42.6	~34.1	β-Mo_2C + C + trace η-MoC_{1-x}	n.d.	η-MoC_{1-x} and completely decomposed

* Alloys homogenized for 30 hrs at 1550°C prior to quenching

** Sample of run number 4

↓ Tin-Quenched

The decomposition of the cubic high temperature phase proceeds with higher velocity than that of η-MoC_{1-x} and the phase can be retained in pure form only by severe quenching of specimens from above 2000°C. The lattice parameters of the phase, measured on two alloy series which were quenched from 2300°C and 2500°C, show a steady increase from a=4.266 Å at 39.7 At% C to 4.281 Å at 43 At% C, at the upper homogeneity limit at the α-MoC_{1-x} + C eutectic isotherm (Figure 30). The eutectoid point, located by combination of DTA (Figures 31 and 32) and chemical analytical studies, lies at 40.4 $\pm$ 0.4 At% C and at a temperature of 1960 $\pm$ 20°C. The decomposition is initiated by oriented intragranular nucleation and subsequent growth of the newly formed phases (Figure 33).

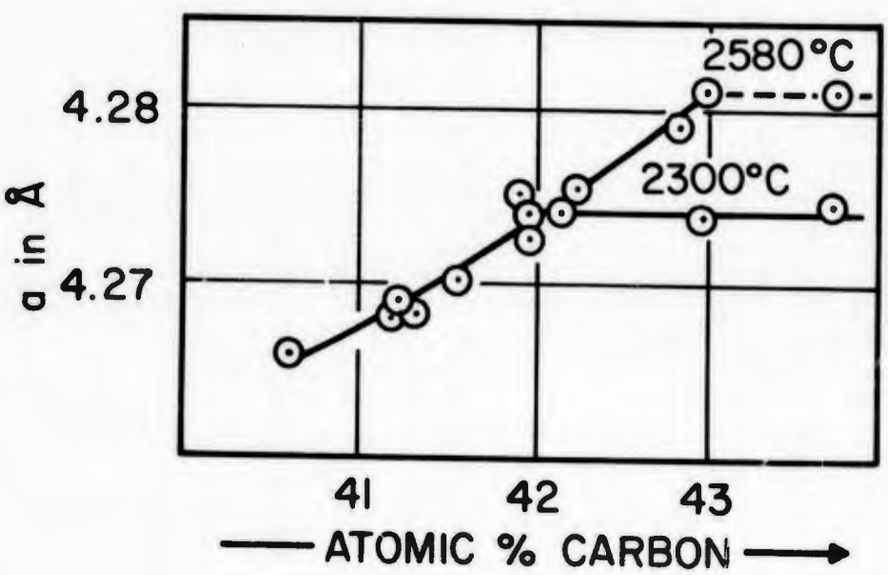

Figure 30. Lattice Parameters of α-MoC_{1-x}. (Tin-Quenched Alloys).

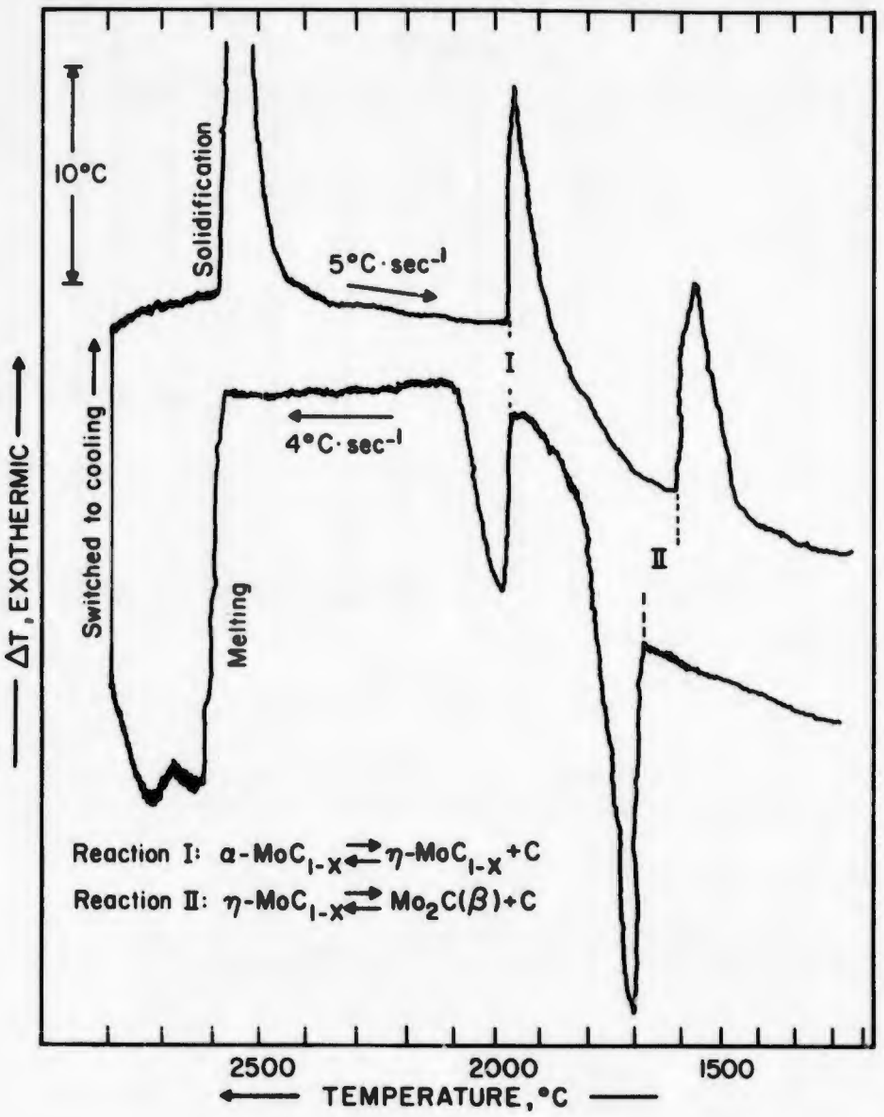

Figure 31. DTA-Thermogram of an Alloy Containing 44 Atomic Percent Carbon.

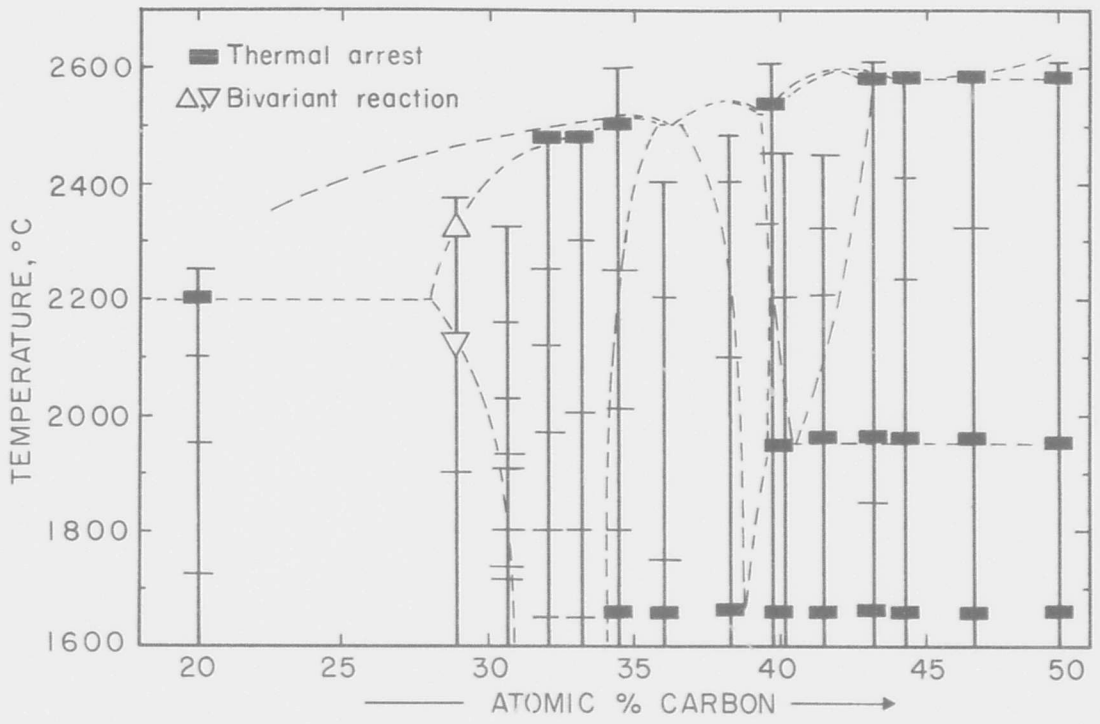

Figure 32. Summary of Differential-Thermoanalytical Studies in the Molybdenum-Carbon System.

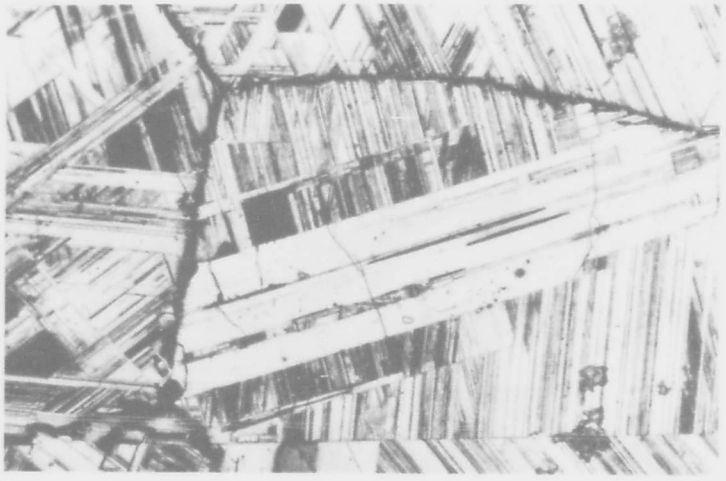

Figure 33. Mo-C (41 At% C), Cooled at 40°C per Second from 2300°C. X250

Subgrain Decomposition of α-MoC_{1-x}
X-ray Analysis: η-MoC_{1-x}, Little α-MoC_{1-x} and Mo_2C.

As was the case for Mo_2C, the rate-determining steps in the decomposition of the η-MoC_{1-x} as well as of the α-MoC_{1-x} phase also seem to be the nucleation of graphite: The decomposition reaction was observed to proceed more rapidly in alloys containing excess graphite, and microscopic examination revealed, that these graphite particles act as centers for the initiation of the decomposition process (see, for example, the micrograph in Figure 34 a). The detailed decomposition processes, however, are very much more complicated. For example in the decomposition of α-MoC_{1-x} it was noticed that alloys cooled at rates between 20 and approximately 60°C per second invariably showed the presence of η-MoC_{1-x}, besides the equivalent amount of free graphite; on the other hand, for alloys cooled at speeds varying between approximately 60 and 150°C per second, significant amounts of $Mo_2C(\beta)$ and free graphite were found to be present. These findings do indicate, that the initial nucleation and growth process does not yield the equilibrium phase η-MoC_{1-x} but forms Mo_2C first. The overall process presumably proceeds as a consecutive reaction according to

$$\alpha\text{-}MoC_{0.69} \xrightarrow{k_1} MoC_{\sim 0.50} + 0.19C \quad (a)$$

$$MoC_{\sim 0.50} + 0.14C \xrightarrow{k_2} \eta\text{-}MoC_{0.64} \quad (b)$$

with the rate constant k_1 being greater than k_2.

Although, for obvious reasons, no well defined reaction temperature can be expected for reaction (b), the temperatures at which the maximum enthalpy changes occur for both processes are clearly resolvable in derivative thermograms taken at intermediate cooling speeds (Figure 35); this behavior is to be expected, if both rate constants are very different.

The close structural relationships between α-MoC_{1-x} and η-MoC_{1-x} further did not rule out completely the possibility for the existence of a critical solution temperature between both phases at temperatures close to melting. As a result of the narrow compositional spacing of both phases, high temperature quenching experiments were indecisive. In order

Figure 34(a) 2550°C X1000

α-MoC_{1-x} and Small Amounts of Excess Graphite. Striae Show Incipient Decomposition.

Figure 34(b) X1000

Alloy Reequilibrated at 1720°C and Quenched. η-MoC_{1-x} (Initial Stages of Decomposition), and Excess Graphite at the Grain Boundaries.

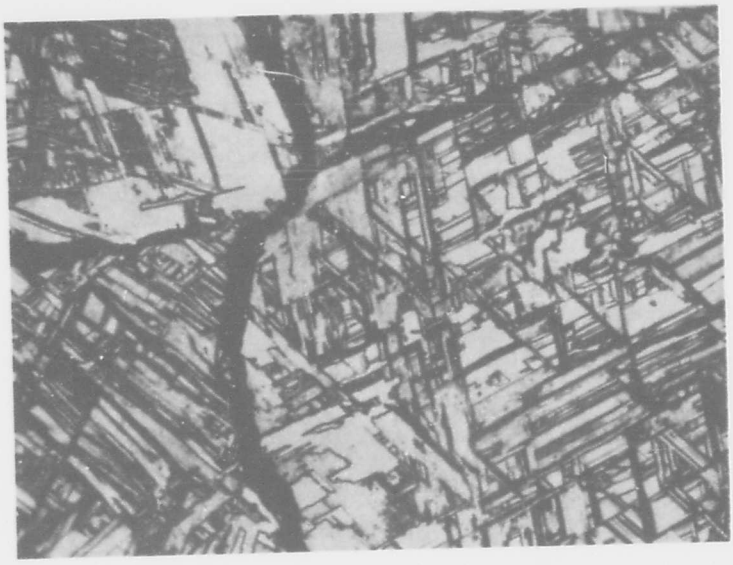

Figure 34(c) X1000

Alloy Reequilibrated at 1600°C, and Quenched.

Decomposition Structure of η-MoC_{1-x}. Note Agglomeration of Graphite at the Grain- and the Subgrain Boundaries.

Figure 34. Microstructures in a Mo-C (43.8 At% C) Alloy After Quenching from 2550°C (a), 1720°C (b), and 1600°C (c).

to establish a more definite answer, diffusion couples consisting of η-MoC_{1-x} and graphite were prepared and allowed to interact for 15 minutes at 2330°C and 2480°C, respectively. The choice of η-MoC_{1-x} as base component in the couple, instead of molybdenum, was given preference, since the rapid diffusion rates in the lower-carbon phases generally prevented the α-MoC_{1-x} phase from growing into a layer of sizeable thickness.

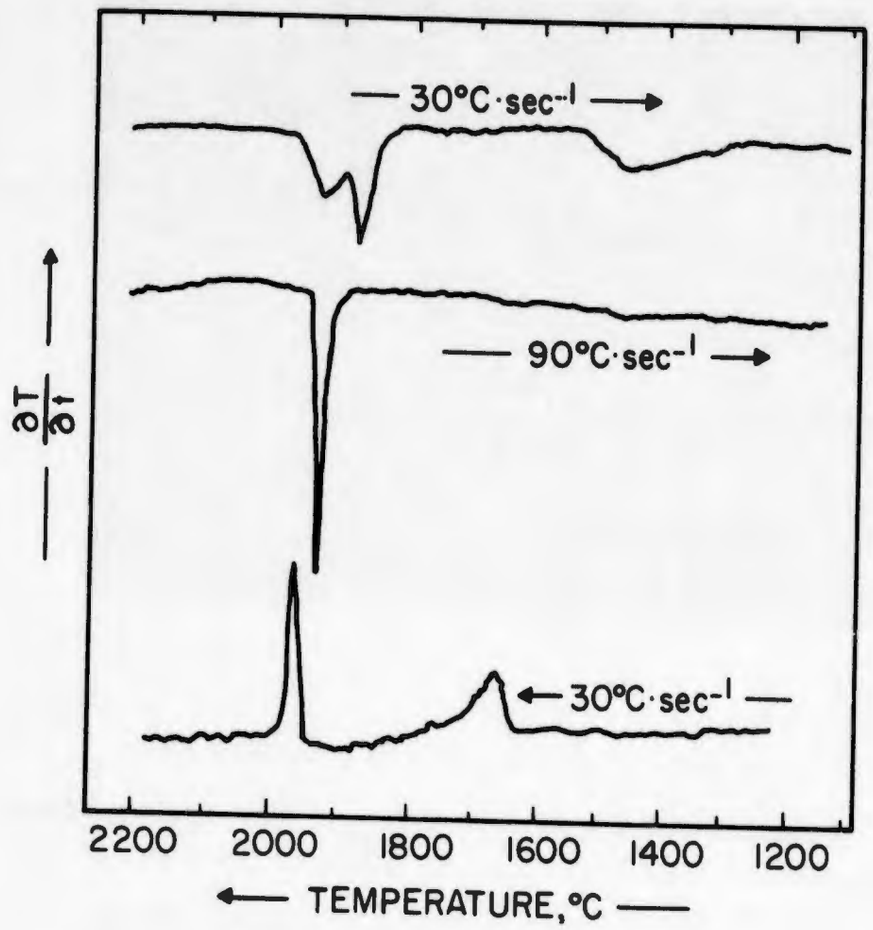

Figure 35. High Speed Derivative Thermal Analysis Experiments on a Mo-C Alloy with 40.6 Atomic Percent Carbon.

In all samples prepared and studied, a clearly distinct reaction zone of α-MoC_{1-x} had formed between the η-phase and graphite (Figure 36). Although the interface between both phases turned out to be quite irregular and partially interleaved, the individual grains are clearly distinguishable by their characteristic decomposition structures (Figure 37). Combining this experimental evidence with the results of the DTA and the melting point studies, we may regard the existence of a small, but finite concentration gap between both phases as established.

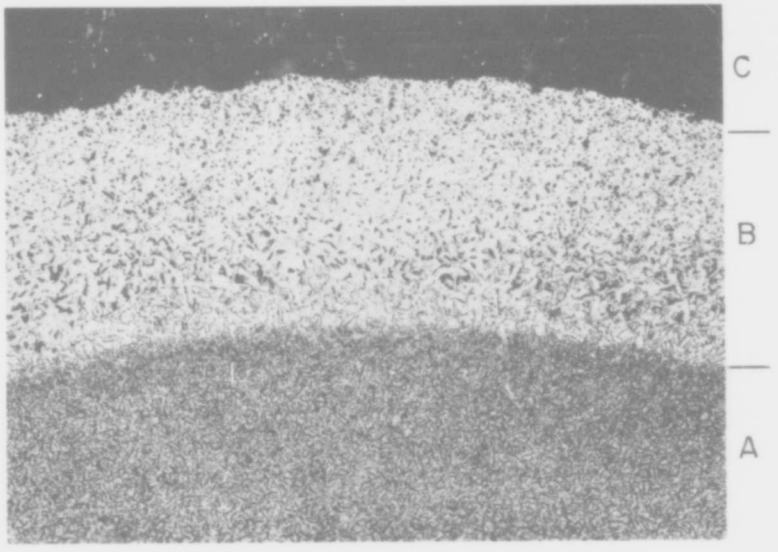

X25

Figure 36. Diffusion Couple η-MoC_{1-x} (39 At% C) + Graphite After 15 Minutes at 2480°C.

Zone A: η-MoC_{1-x}, Partially Decomposed.
Zone B: α-MoC_{1-x}, Decomposed into η-MoC_{1-x} and Graphite.
Zone C: Graphite.

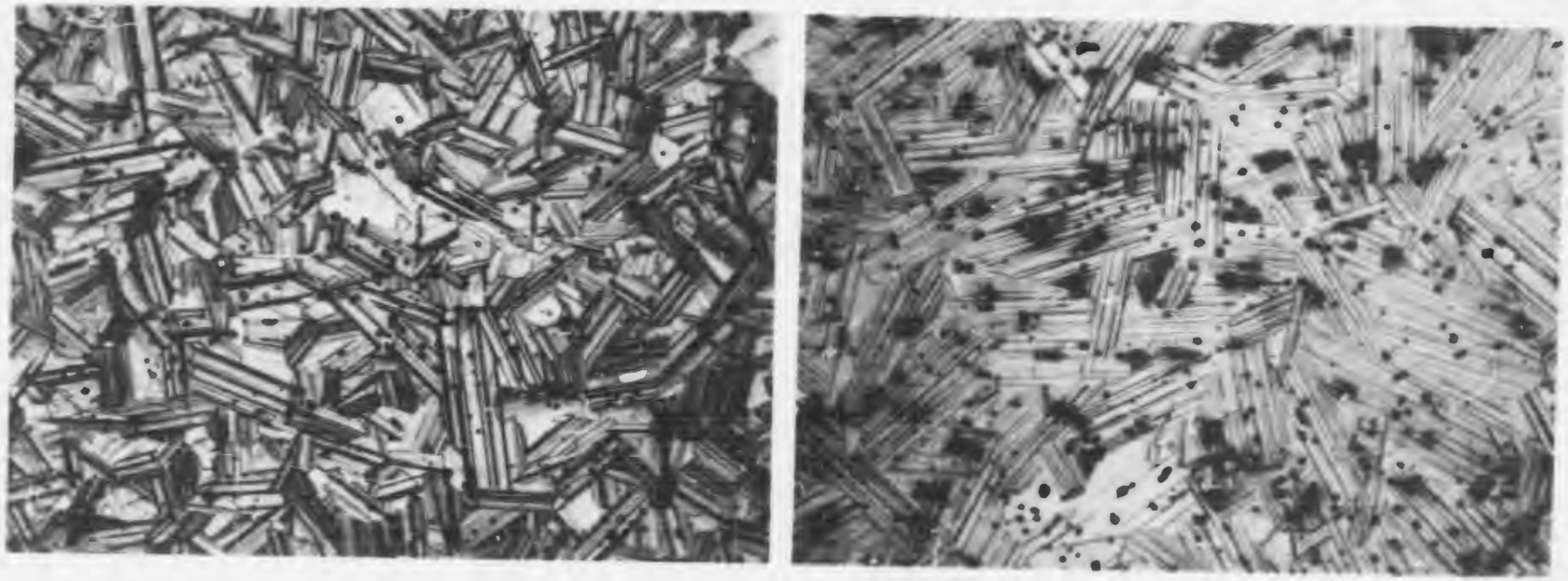

37(a) X400

Zone A, Partially Decomposed η-MoC_{1-x}

37(b) X400

Zone B, Decomposed α-MoC_{1-x}

Figure 37. Microstructure of the Core (a) and the Reaction Layer (b) in the Diffusion Couple Shown in Figure 36.

For the experimental determination of the composition of the carbon-saturated melts, alloys having initial carbon contents between zero and 40 atomic percent were equilibrated with graphite. The samples were held molten for approximately 20 minutes at the chosen equilibrium temperature, and then force-filtered through porous graphite plugs and quenched in order to avoid segregation of the lower density graphite from the melt. Each experiment was carried out in duplicate, and the samples were analyzed after the runs. The results are summarized in the diagram shown in Figure 38.

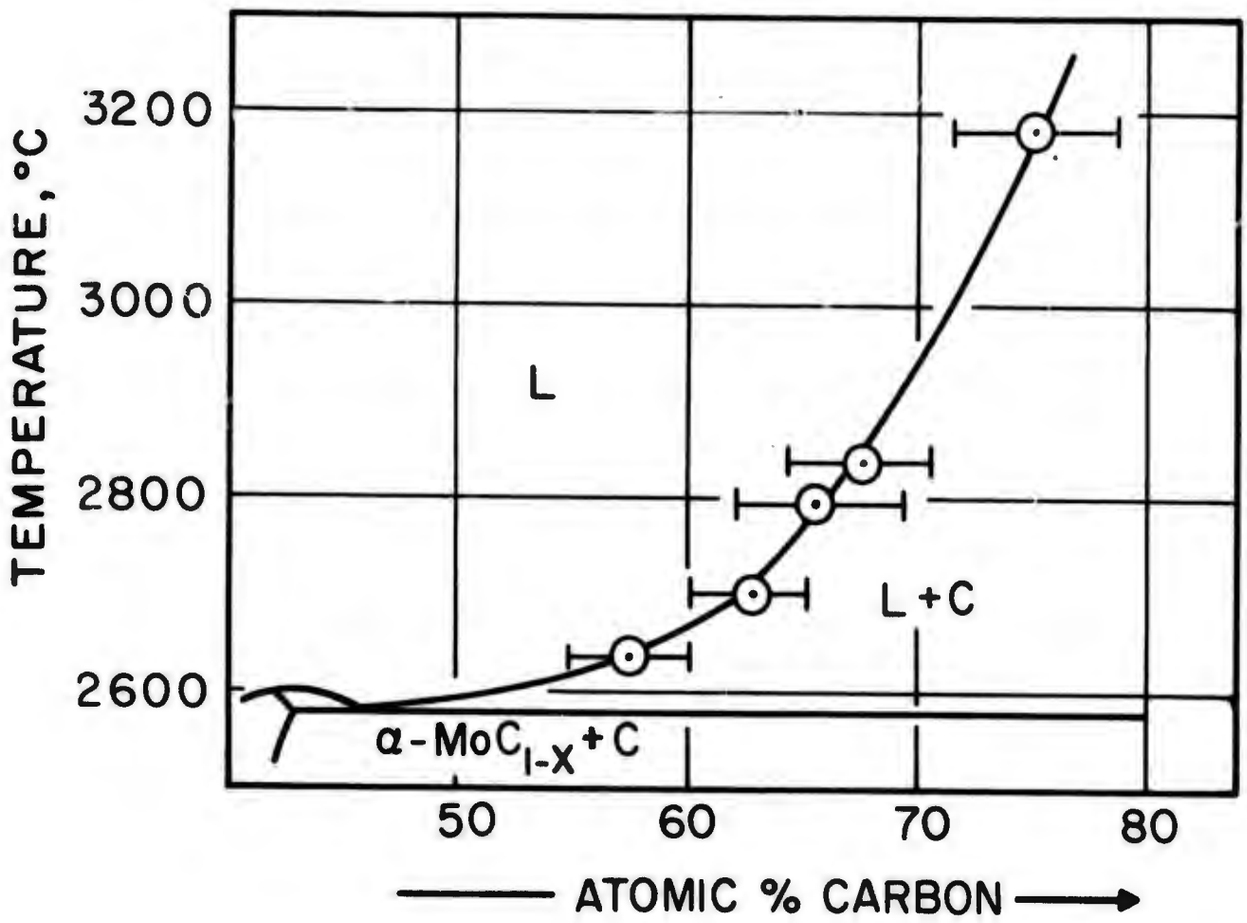

Figure 38. Composition of the Carbon-Saturated Melt as a Function of Temperature.

E. ASSEMBLY OF THE PHASE DIAGRAM

The experimental data have been combined to yield the constitution diagram depicted in Figure 39. For the order-disorder transition in Mo_2C, we propose a first order transition, and consequently the existence of a singular point in the diagram, at 32.5 At% C and a temperature of 1430 $\pm$ 10°C. At this point, ordering of the interstitial sublattice and the displacive transformation, leading to an orthorhombic distortion of the hexagonal close-packed metal host lattice, occur simultaneously. In

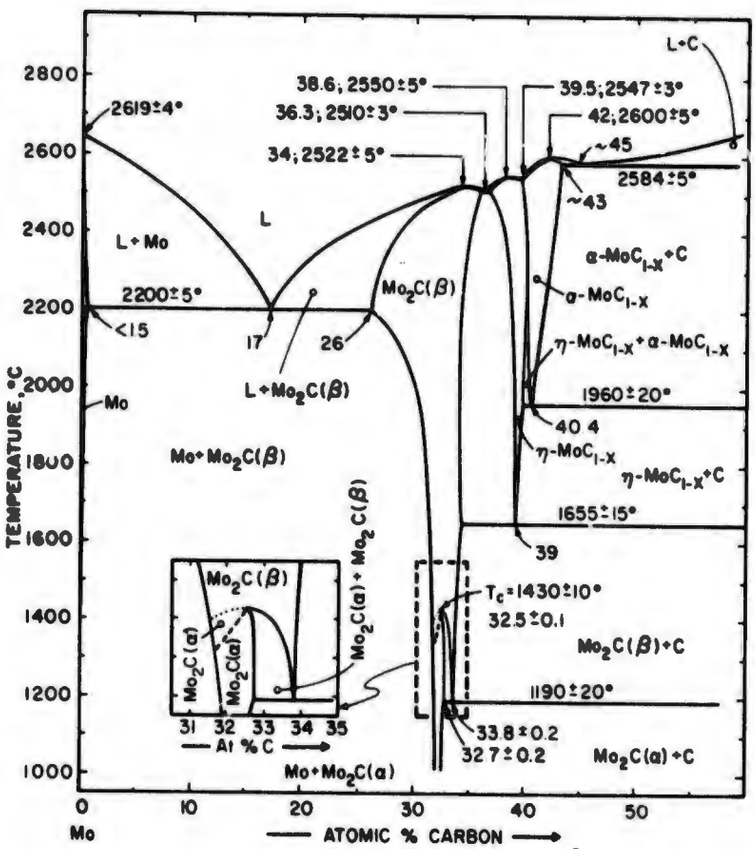

Figure 39. Proposed Constitution Diagram for the Molybdenum-Carbon System.

(Temperature Figures Based on Reproducibility.)

lower carbon alloys, the order-disorder transition is separated by a small, but distinguishable, temperature gap from the displacive transformation. Both transitions are assumed to be of the second order and to proceed without phase discontinuity. As a consequence, no reaction isotherms are shown in the Mo + Mo_2C region of the system. At concentrations above 32.5 At% C the transition in Mo_2C is two-phased, and the disordered, hyperstoichiometric $Mo_2C(\beta)$-phase finally terminates in a eutectoid (pseudomonotectoid) reaction isotherm at 1190°C.

The hexagonal (pseudocubic) η-MoC_{1-x} and the cubic (B1) α-MoC_{1-x} are shown as distinct phases up to their respective melting range, forming a degenerate eutectic equilibrium at 2547°C.

IV. DISCUSSION

The newly established phase diagram differs appreciably from the previously accepted system, and especially large differences were noted for the solid state equilibria, including the observation of a previously undiscovered order-disorder transition of Mo_2C. Previous work also failed to provide consistent temperature data for the stability ranges for the cubic and hexagonal high temperature phases. In view of the considerable scatter of the melting temperatures reported for the intermediate phases, a detailed assessment and a comparison of previous data with our temperature values, appears as difficult. Better agreement was obtained for the temperatures of certain melting isotherms where our measurements corroborate previous data by W. P. Sykes et al.[19], and M. R. Nadler and C. P. Kempter[20] concerning the Mo + Mo_2C eutectic temperature, and the recent determination of the α-MoC_{1-x} + C eutectic line by T. C. Wallace, et al.[15].

Concerning the thermodynamic stability of the high temperature phases η-MoC_{1-x} and α-MoC_{1-x}, we may use the observed phase relationships in conjunction with the known thermodynamic quantities for Mo_2C to derive approximate expressions for their free energies of formation.

At the eutectoid reaction isotherm at 1655°C, the free energy change of the reaction

$$\eta\text{-}MoC_{0.64} \longrightarrow MoC_{\sim 0.5} + 0.14\,C$$

is zero; hence, for that particular temperature, we obtain

$$\Delta G_{f,\,MoC_{0.5}} = \Delta G_{f,\,\eta\text{-}MoC_{1-x}} \qquad (T = 1928\,°K)$$

From the data recently compiled and evaluated by L.B. Pankratz, et al.[31], the free energy of formation of Mo_2C can be approximated for the temperature range above 1400°K with sufficient accuracy by the expression

$$\Delta G_{f,\,MoC_{\sim 1/2}} \simeq -4,750 - 1.36\,T \text{ [cal/gr.-At.Mo]}$$

yielding for the free energy of formation of $\eta\text{-}MoC_{1-x}$ at 1928°K,

$$\Delta G_{f,\,\eta\text{-}MoC_{1-x}} \simeq -7370 \text{ [cal/gr.At.Mo.]}$$

Assuming the same temperature dependence of the free energy of formation of $\eta\text{-}MoC_{1-x}$ as for Mo_2C, we obtain as lower limit for the free energy of formation of the cubic high temperature at the eutectoid reaction isotherm at 1960°C (2233°K):

$$\Delta G_{f,\,\alpha\text{-}MoC_{1-x}} \leq -7780 \text{ [cal/gr.At.Mo.]}$$

Because, however, the reaction to form the η-phase from Mo_2C and carbon involves a sizeable enthalpy change, the corresponding positive entropy consequently will result in a somewhat more negative temperature-dependent term as in the expression for Mo_2C. From data derived from phase equilibria in ternary metal carbon systems[2], and incorporating the more precise values determined in this work for the isothermal reaction temperatures,

the free energy of disproportionation of η-MoC_{1-x} into Mo_2C and carbon becomes:

$$\Delta G_R = \Delta G_{f,\,MoC_{1/2}} - \Delta G_{f,\,\eta\text{-}MoC_{1-x}} = -635 + 0.33\ T\ [cal/gr.At.Mo],$$

yielding for the free energy of formation of η-MoC_{1-x}

$$\Delta G_{f,\,\eta\text{-}MoC_{1-x}} \simeq -4,115 - 1.69\ T\ [cal/gr.At.Mo] \qquad (1)$$

This expression can now be used to derive the free energy of formation of α-MoC_{1-x} at the eutectoid decomposition temperature. Insertion of the equilibrium temperature into equation (1) yields immediately

$$\Delta G_{f,\,\alpha\text{-}MoC_{1-x}} \simeq -7,890\ [cal/gr.At.Mo] \quad (T = 2233°K)$$

Combining this value with quantities calculated from the observed temperature dependence of the homogeneous ranges of the B1-phase in ternary metal-carbon systems[2], we obtain as temperature-dependent expression for the free energy of formation of the cubic high temperature phase,

$$G_{f,\,\alpha\text{-}MoC_{1-x}} \simeq -2,200 - 2,55\ T[cal/gr.At.Mo] \qquad (2)$$

The free energy of formation of the α-MoC_{1-x} phase as its isothermal decomposition temperature, based on the known data for Mo_2C, falls within the range of -6 to -9 kcal per gram-atom molybdenum derived earlier from the phase-relationships in the Nb-Mo-C System[14]. A value of -2.6 ± 1.5 kcal/mole over the range 1720 - 2370°K, based on a similar evaluation of the phase relationships in the Zr-Mo-C system[15], is incompatible with the phase relationships in the molybdenum-carbon binary.

The most interesting feature, no doubt, concerns the phase phenomena associated with the order-disorder transition in Mo_2C. Neglecting, for the sake of discussion, the changes introduced by the distortion of the hexagonal or pseudohexagonal lattice, we observe that the feature of alternating

carbon-hole occupancy along the hexagonal c-axis (a-axis in the orthorhombic setting) is common to all ordered structures of the Me_2C-phases (Figure 40). We may argue, that in order to minimize the strain energy of the lattice at a given total semimetal concentration, sites in the immediate neighborhood of already occupied interstitial lattice positions become less favored, i.e, require an extra amount of energy for their occupation. Specifically for the Me_2C-lattice, once one of the two octahedral sites (A-sites, either in layer 0 or 1/2 in the hexagonal cell) is filled, occupation of the other

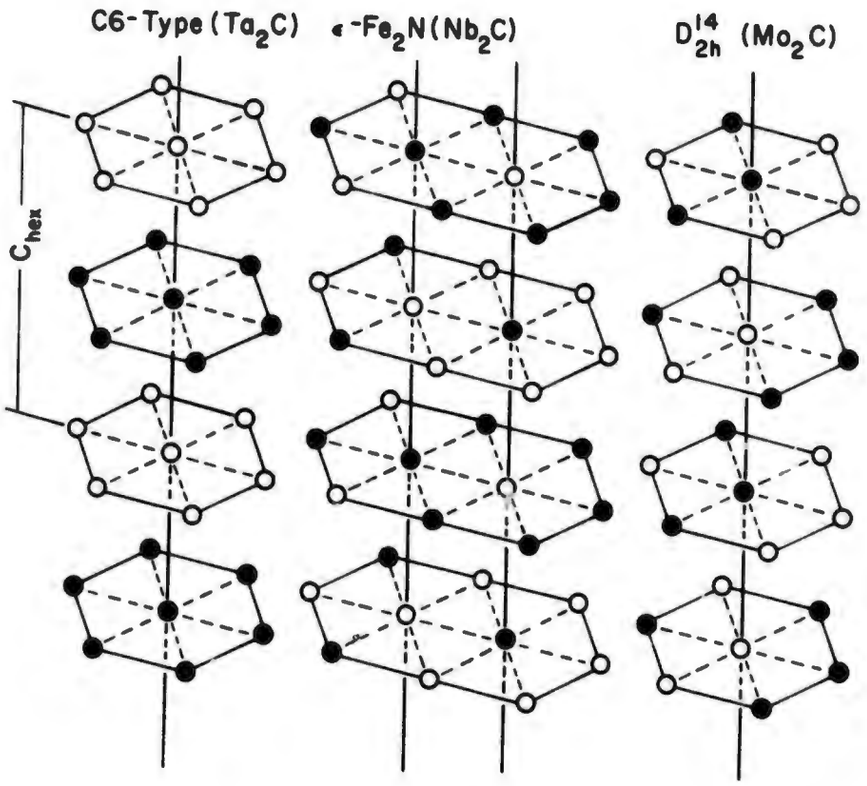

Figure 40. Carbon-Hole Coordination Types in Me_2C Order Structures.

Filled Circles: Carbon Atoms
Open Circles: Vacancies

octahedral site having the same basal coordinates, but at half the c-spacing from the already occupied site, would become accessible only by expenditure of an amount of energy ΔE in excess of that required for the occupation of a lattice site of the first kind. Hence, substantial occupation of the unfavored (B-sites), which must necessarily occur at hyperstoichiometric compositions, will tend to affect mainly the c-spacing in the lattice, since a new layer of carbon atoms has to be accommodated, while the conditions in the layers perpendicular to the c-axis remain essentially unchanged. That these conditions prevail, is essentially substantiated by the observed course of the lattice parameters with varying carbon content (Figure 18).

However, for the ordering reaction to occur, some interaction between atoms of neighboring chains also has to exist, for it has been shown[32], that long range order along a linear chain of alternating atoms cannot exist at temperatures above absolute zero. Which type of order structure will prevail will, of course, be dependent upon the relative magnitude of the interactions within the host atom lattice and of the disturbances created by the incorporation of the interstitial atoms. As an example, in parent lattices with high lattice energies and favorable size factors, the C6-type structure, characterized by the occurrence of only like neighbor (hole-hole and carbon-carbon) pairs in the (00ℓ) planes seem to be favored (Figure 40), whereas the tendency to form the maximum possible number of unlike neighbor pairs along the c-axis as well as in the layers parallel to the basal plane is pronounced in metal lattices with lower lattice energies and less favorable size factors. An example, where these principles are followed, is the ordered structure of Mo_2C.

Besides the tendency to form the maximum number of unlike neighbor pairs in the latter cases, one may expect that in order to minimize the lattice strain, the distribution of like and unlike pairs in alternating layers should be as even as possible. We may define the nonuniformity in the number of like neighbor pairs within the layers by the parameter

$$A = \frac{n_{c\text{-}c} - n_{h\text{-}h}}{n_{c\text{-}c} + n_{h\text{-}h}}$$

where n_{c-c} and n_{h-h} denote the number of carbon-carbon and hole-hole pairs within the unit cell. We find, that the C6- and ϵ-Fe_2N-type exhibit maximum nonuniformity, corresponding to A = 1, whereas the Mo_2C-type shows an even (A = 0) distribution of like neighbor pairs in the (00ℓ) planes.

Following the above principles as a guide, and considering only nearest neighbor interactions, other energetically closely equivalent patterns can be constructed. Model I in Figure 41 corresponds to the ϵ-Fe_2N-type, proposed by N. Terao[33] for the order-structure in Nb_2C; it has, according to the definition above, a nonuniformity factor of A = 1. Model IV has a nonuniformity factor of A = 0.75, whereas patterns II and III have A = 0. Pattern III is of special interest; apart from being energetically equivalent to the Mo_2C-type, the symmetry elements also lead to the same characteristic space-group, namely D_{2h}^{14} - Pbcn. Although further confirmation by neutron diffraction techniques must be awaited, this, or a closely related structure, seems to be exhibited by the lower temperature modifications for Nb_2C and V_2C[34].

In view of the close similarities between the various structural patterns it is also conceivable, that associated with slight variations in stoichiometry and purity as well as in the specimen preparation, a variety of different but related sublattice order-structures may be formed for the same phase. As an example, an investigation of the thermal behavior of the W_2C indicated two transitions, of which one, occurring at 2450°C, was identified earlier[3, 35] as being due to disordering in the carbon sublattice. The nature of the second transformation is not fully resolved yet, but indications are, that it involves only a transition between two different types of ordered structures. For W_2C a structure which is ordered according to the C6-type has been proposed previously by L.N. Butorina and Z. G. Pinsker[36]. Although the higher lattice energy of the metal will tend to override the effects of the secondary coordination of interstitial atoms in the basal planes, it would seem from the foregoing considerations, that as a result of the comparatively small atomic diameter of tungsten, structures other than the C6-type are expected to have increased stability at lower temperatures.

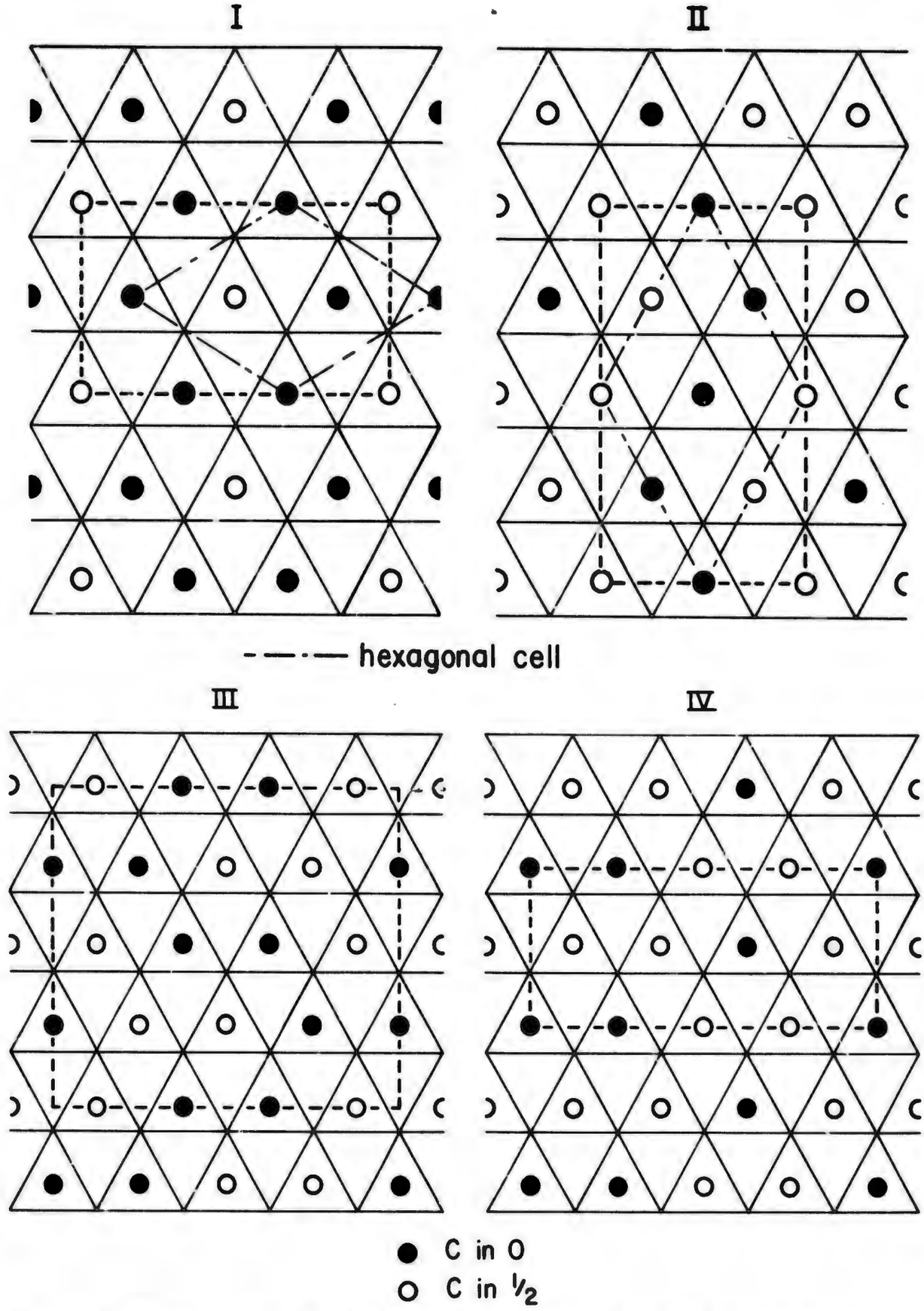

Figure 41. Energetically Equivalent Layer Patterns for Me_2C Order Structures. The Metal Atom at z=1/4 at the Vertices of the Triangles, and at z=3/4 at the Centers of the Empty Triangles are Omitted.

Examining the order-disorder transition in Mo_2C, we observe from the volume relationships in the alloy series cooled at approximately 100°C per second from 1350°C and 2300°C (Figure 42), that the basic ordering process at substoichiometric compositions must proceed with comparatively high speed. Furthermore, since the unit cell volumes of the orthorhombically distorted lattice fall on the same line as those computed for the pseudohexagonal cell, we have to conclude, that the displacive transformation is a secondary phenomena to the ordering process, i.e. its appearance is bound to the a priori existence of a certain degree order in the lattice.

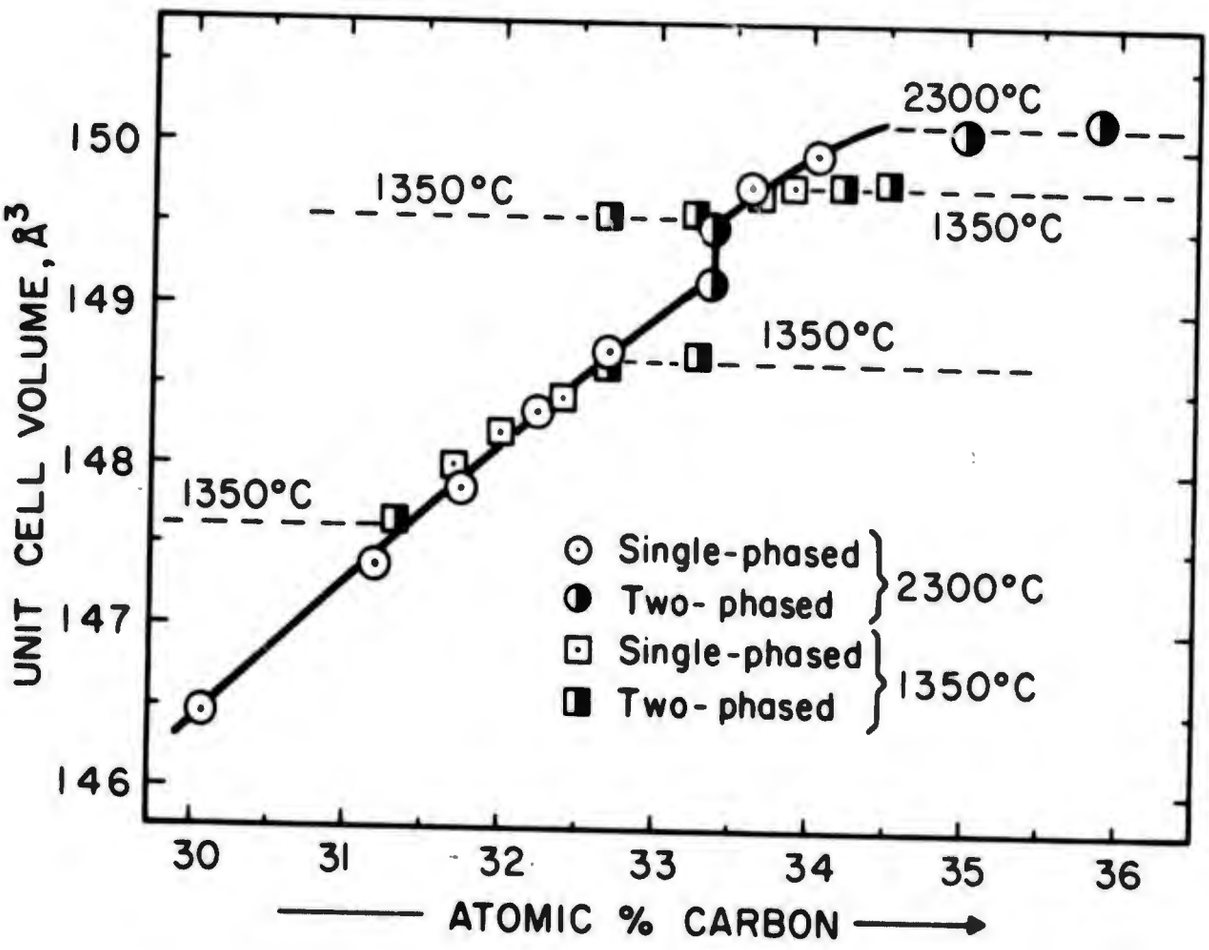

Figure 42. Unit Cell Volume of Mo_2C Alloys.
(Cooled from the Indicated Temperatures at Approximately 100°C per Second).

From the data obtained from the rapidly quenched alloy series (Figure 18) we further deduce from the anomalous course of the lattice dimensions, that, up to approximately 32.5 At% C, very few carbon atoms enter into energetically unfavored positions along the c-axis; however, as soon as the stoichiometric composition is approached, corresponding vacancies are no longer available, and additional carbon atoms are forced to enter vacant positions between carbon atoms in the linear chains along the prism axis. As a result, the structure is incapable of reverting from the disordered into the ordered state, in spite of the ordering forces exerted by the atoms in neighboring chains.

Considering possible atom transfer reactions within the ordered Mo_2C structure (Figure 43), the total enthalpy change in process (1) is given

$$\Delta H_1 = - (2V_c - V_a)$$

where V_c stands for the expression $2H^{(c)}_{c-h} - H^{(c)}_{c-c} - H^{(c)}_{h-h}$ and V_a for $2H^{(a)}_{c-h} - H^{(a)}_{c-c} - H^{(a)}_{h-h}$. The terms $H^{(c)}$ and $H^{(a)}$ are, respectively, the heats of formation of corresponding pairs along the c-axis, and within the (00ℓ) planes.

Shifting a carbon atom within neighboring positions along the c-axis (process 2 in Figure 43), yields, in case of the ordered Mo_2C lattice, an enthalpy change of

$$\Delta H_2 = - (V_c - 2V_a)$$

Since, as a result of the closer spacing, we expect V_c to be much more negative than V_a, the probability of occurrence of process 2 will be larger than that of process 1.

Consider now the effect of vacant A-sites, which can occur as a result of a transfer reaction according to process 1 or 2, or, preferably, by carbon deficiencies in the lattice. A simple enumeration of broken and newly formed

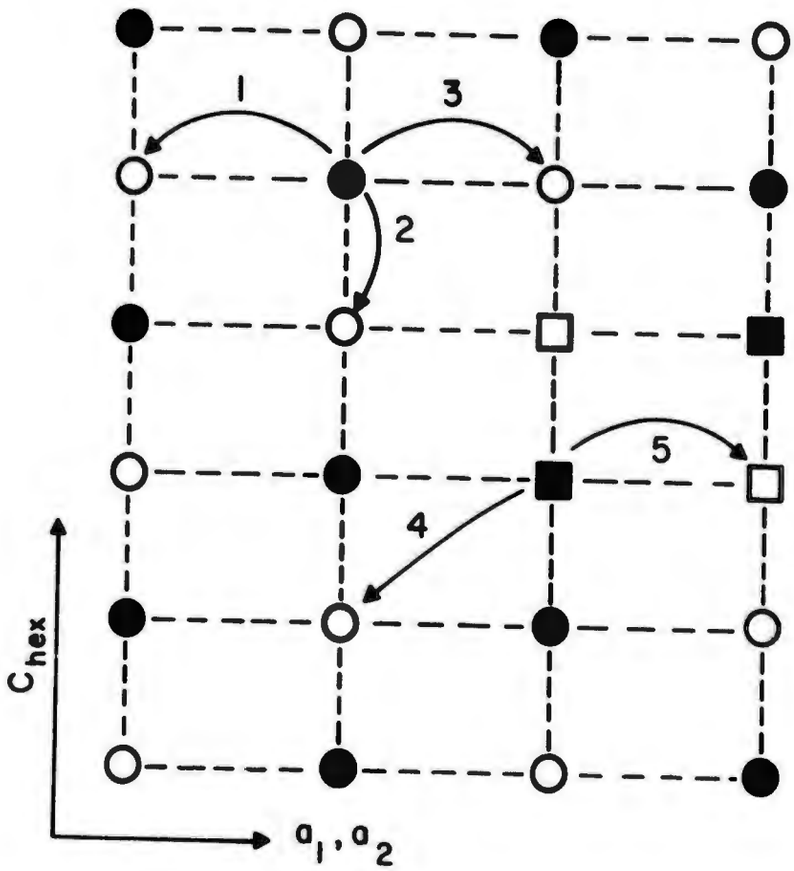

Figure 43. Diagrammatic Presentation of Carbon Transfer Reactions in the Mo_2C-Lattice.

pair bonds reveals, that the enthalpy change for the transfer of a carbon atom to a neighboring chain vacancy, such as shown for process 3, is reduced to

$$\Delta H_3 = - (V_c - V_a)$$

Since, as discussed before, V_c is considered to be much more negative than V_a, this enthalpy change is of the same order of Magnitude as ΔH_2, i.e., the energy required to transfer a carbon atom into neighboring positions

within the chain. Thus, the existence of extra vacancies in the deficient carbide increases the number of energetically equivalent positions, but, more important, allows transfer reactions between neighboring chains at a much lower energy level than is possible in the stoichiometric or hyper-stoichiometric carbide. The ultimate effect of the possibility for chain-chain interactions in the substoichiometric carbide is that ordering can be achieved by simple transfer reactions, allowing preordered chain pieces to coher into long range order at the transition temperature.

To a first approximation, and not counting multiple interchange reactions for the formation of suitable vacancies, we may arrive at an appropriate figure for the enthalpy change, if we submit that the maximum carbon content where ordering can occur, will be given by the conditions, that the number of vacancies should, approximately, equal the number of double pairs. In the Mo_2C structure a vacancy is shared by four atoms; hence, we can formulate the above condition as

$$4n_{vac} \approx n_{c-c-c}$$

where n_{c-c-c} denotes the number of double pairs of carbon atoms. Expressing the gross composition of the phase as MoC_y, the number of extra vacancies ($y < 1/2$) becomes

$$n_{vac} = \frac{N}{2} - y.$$

The distribution of carbon atoms and vacancies among the two types of interstitial lattice sites is given by[26]

$$RT \ln K = \Delta E,$$

where ΔE denotes the free energy change in transferring one gram atom of carbon atoms from A to B sites, and K stands for the expression

$$K = \frac{x_{c\alpha}}{x_{\alpha}} \cdot \frac{x_{c\beta}}{x_{\beta}}$$

$x_{c\alpha}$, x_{α} mole fraction of carbon atoms and of vacancies on A-sites

$x_{c\beta}$, x_{β} mole fraction of carbon atoms and of vacancies on B-sites

For compositions close to stoichiometric, y is approximately equal to 1/2 and the distribution equation is separable into[26]

$$RT \ln \frac{x_{c\alpha}}{x_{\alpha}} = RT \ln \frac{x_{\beta}}{x_{c\beta}} \simeq \frac{\Delta E}{2}$$

Since we may set $x_{c\beta}$ equal to x_{α}, the number of vacancies in terms of the overall compositions can be expressed as

$$x_{vac} = \frac{2n_{vac}}{N} = 1-2y,$$

we finally obtain the condition:

$$4(1-2y) = \frac{1}{1+\exp\left[-\frac{\Delta E}{2RT}\right]}$$

According to the phase diagram, the maximum carbon content at which ordering occurs is 32.5 At% C. Substitution of $1-2y = 0.0372$ into the above equation yields

$$\Delta E \simeq \Delta H_1 = -(2V_c - V_a) \simeq 12,000 \text{ cal.}$$

For the ordering process in substoichiometric compositions, we may, because of the lower energies involved, choose reaction 2 or the energetical equivalent interchain transfer as the relevant process, i.e.,

$$\Delta E \approx \Delta H_2 = -(V_c - V_a)$$

From the equation relating the ordering temperature to the energy quantities and to the stoichiometry[37],

$$T_c = \frac{Z\Delta H_2(1-y)y}{R}$$

we obtain, inserting a coordination number of $Z \approx 2$, and $y \approx 1/2$,

$$\Delta H_2 \approx -2RT_c \approx 6800 \text{ cal}$$

i.e. approximately half the value of ΔH_1, as would be expected from the previously made assumption of $V_c \ll V_a$. With this energy parameter, the above equation predicts a decrease of 10°C in the Curie temperature as the low carbon boundary of the phase is approached.

Long range order apparently cannot prevail at hyperstoichiometric compositions, and upon passing through a critical temperature range, the homogeneous structure decomposes into two distinct phases, of which one has a substoichiometric composition and shows long range order while the other is hyperstoichiometric and exhibits no long range coherence in the interstitial sublattice. Considering that the reaction mechanism involved in the disproportionation of the homogeneous phase, the energetically most favorable and hence most likely process is the interchain transfer of carbon atoms, i.e. carbon atoms in B-position in one chain are transferred into a energetically equivalent or closely equivalent position in neighboring chains. Growth of the new phases, according to this reaction scheme, should, therefore, occur in directions perpendicular to the (000ℓ) direction in the hexagonal cell; this behavior seems to be confirmed by recent studies of the orientation of the veining structure in single crystal dimolybdenum carbide[38]; in this connection, it is interesting to note, that in the proposed growth direction $\langle 2\bar{1}\bar{1}0\rangle$ the carbon atoms and vacancies form alternating, and nearly perfect planar sheets; an evaluation of the atomic spacings in the disordered and the ordered modification further reveals that the distances within the $(2\bar{1}\bar{1}0)$ plane undergo only minimal changes and therefore this plane forms the plane of coherence between the coexisting planes.

Because of the lack of precise thermodynamic quantities for the phase in the critical temperature region, the available data do not lend themselves to a detailed thermodynamic description of the observed phase phenomena; nevertheless, the variation of the configurational free energy (Figure 44) shows features, which can be related to the observed disproportionation process[26]. The conditions are further complicated by the occurrence of a

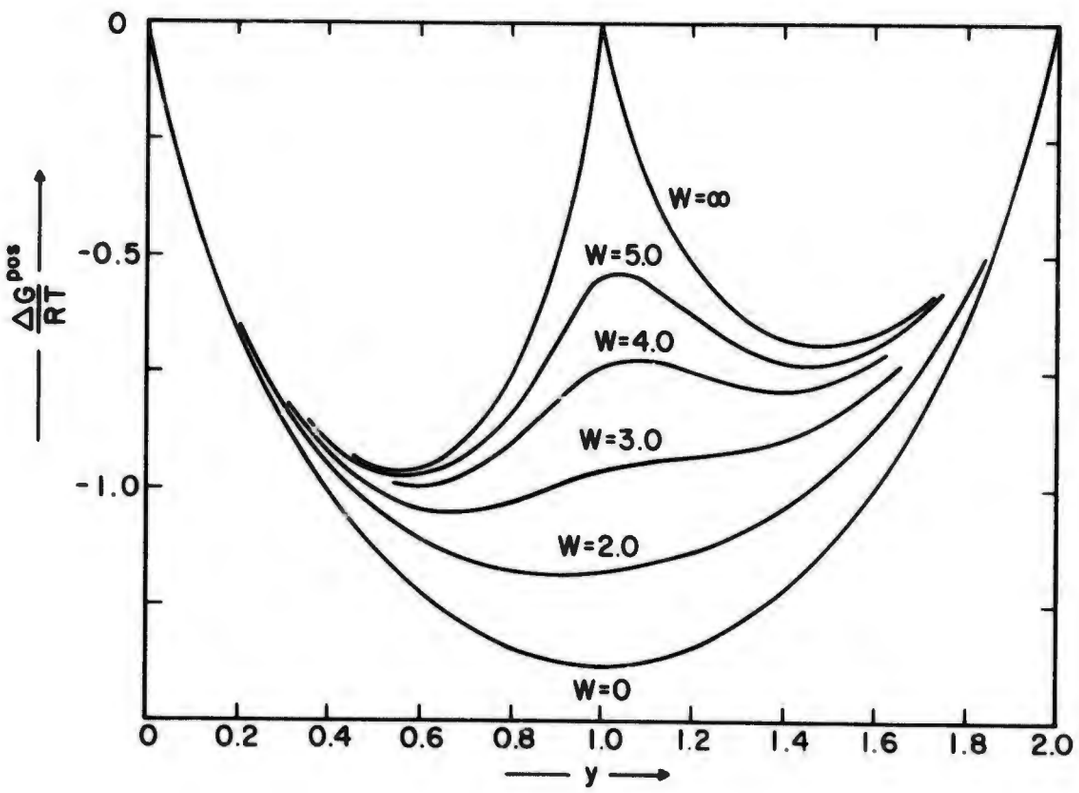

Figure 44. Positional Free Energy Resulting from the Distribution of Interstitial Atoms and Holes Among Two Energetically Different Types of Lattice Sites.

Energy Parameter $W = \frac{\Delta E}{RT}$; Ordinate Values Refer to One Mole Me_2C_y.

displacive transformation, which, from all experimental evidence available, seems to coincide with the ordering temperature at the point exhibiting the highest ordering temperature, whereas it is clearly separated from the ordering reaction at lower carbon contents. One immediate and obvious effect of the distortion of the metal host-lattice is that it enforces the ordering tendency, i.e. the decrease of the long range order parameter with temperature will be less than would be expected from the interaction energies and will become pronounced only in the temperature interval between the displacive transformation and the ordering temperature. Concerning the nature of the displacive transformation, it should be recalled that it it to be considered as a continuous process in a thermodynamic sense, i.e. the free energy curve for the distorted form should merge gradually into that of the undistorted modification. Although, due to the small displacements involved, this point is difficult to prove for Mo_2C by X-ray diffraction methods alone, the gradualness of the reaction is clearly demonstrated in the analogous cases for V_2C and Nb_2C, where the observed degrees of distortion are much larger[34]. In these phases, the displacive transformation proceeds comparatively slow, and states intermediate between the hexagonal or pseudohexagonal form and the maximally distorted indication can be retained by variation of the annealing and cooling conditions.

V. CONCLUSIONS

The binary alloy system molybdenum-carbon contains three intermediate phases Mo_2C, η-MoC_{1-x}, and α-MoC_{1-x}, of which α-MoC_{1-x} and η-MoC_{1-x} are stable at high temperatures only, and Mo_2C undergoes a sublattice order-disorder transformation in the vicinity of 1400°C.

$Mo_2C(\beta)$ has a hexagonal close-packed metal host lattice and no long range order in the carbon sublattice. The homogeneous range of the phase is strongly temperature-dependent, extending at 1700°C from 31.0 At% C (a=2.998 Å, c=4.733 Å) to 34.1 At% C (a=3.011 Å, c=4.771 Å), at 2000°C from 30 At% C (a=2.990 Å; c=4.730 Å), to 34.4 At% C (a=3.010 Å; c=4.778 Å), and at 2200°C from 26 to 34.5 at% C. The congruent melting point is located at 34 At% C and 2522°C. The phase probably shows considerably short range order, approaching only at temperatures close to melting the completely disordered L'3-type.

The alloy composition at 32.5 At% C transforms in a rapid first order transition at 1430°C into the ordered modification (orthorhombic D_{2h}^{14} - Pbcn a=4.733 Å, b=6.042 Å, c=5.202 Å). In compositions with less than 32.5 At% C, the transition is of the second order and proceeds as a homogeneous reaction. Hyperstoichiometric compositions undergo a discontinuous phase change, and the disordered modification decomposes in a slow eutectoid reaction at 1190°C into the ordered form and free graphite.

η-MoC_{1-x} (hexagonal, D_{6h}^{4}-type, a=3.010 Å; c=14.64 Å at 39 At% C) has a congruent melting point at 39 At% C and 2552°C. The phase decomposes eutectoidically at 1655°C and 39 At% C into $Mo_2C(\beta)$ and graphite.

The cubic (B1) α-MoC_{1-x} melts congruently at 2600°C and a carbon content of 42 At% C. Its homogeneity range extends from 39.7 At% C (a=4.266 Å) to 42 At% C (a=4.274 Å) at 2300°C, and to 43 At% C (a=4.281 Å) at 2580°C. The phase decomposes in a rapid eutectoid reaction at 1960°C and 40.4 At% C into η-MoC_{1-x} and graphite.

REFERENCES

1. U.S. Air Force Contract AF 33(615)-1249. Report Series AFML-TR-65-2, Parts I to IV (28 Volumes, 1964 to 1966).

2. E. Rudy and Y.A. Chang: Plansee Proc., 1964, p.786.

3. H.D. Heetderks, E. Rudy and T. Eckert: Planseeber. Pulvermet. 1965, vol.13, p.105.

4. Compare R. Kieffer and F. Benesovsky, "Hartstoffe" (Wien, Springer, 1963).

5. H. Tutiya: Sci. Pap. Inst. Phys.Chem. Res. Tokyo, 1932, vol.19, p.384.

6. H. Nowotny and R. Kieffer: Metallforschung, 1947, vol. 2, p.257.

7. R.J. Fries and C.P. Kempter: Analyt.Chem., 1960, vol.32, p.1898.

8. E. Parthé and V. Sadagopan: Mh.Chem., 1962, vol.93, p.263.

9. H. Nowotny, E. Parthé, R. Kieffer, and F. Benesovsky: Mh.Chem., 1954, vol.85, p.255.

10. E. Rudy, El. Rudy, and F. Benesovsky: Planseeber.Pulvermet., 1962, vol.10, p.42.

11. E.V. Clougherty, K.H. Lothrop, and J.A. Kafalas: Nature, 1961, vol. 191, p. 1194.

12. K. Kuo and G. Hägg: Nature, 1952, vol. 170, p.245.

13. A. Westgren and G. Pharagmen: Z.anorg.allg.Chemie, 1926, vol.156, p.27.

14. E. Rudy, F. Benesovsky, and K. Sedlatschek: Mh.Chem. 1961, vol.92, p.841.

15. T.C. Wallace, C.P. Guitierrez, and P.L. Stone: J.Phys.Chem., 1963, vol.67, p.796.

16. J.L. Lander and L.H. Germer: Am.Inst.Min.Met.Eng.Techn. Pub. Nr. 2259 (1947).

17. L.C. Browning and P.H. Emmett: J.Am.Chem.Soc., 1952, vol.84, p.4773.

REFERENCES (Cont'd).

18. I.F. Ferguson, J.B. Ainscough, D.Morse, and A.W. Miller: Nature, 1964, vol.202, p. 1327.

19. W.P. Sykes, K.R. VanHorn, and C.M. Tucker: Trans.Am.Inst. Min.Met.Eng., 1935, vol. 117, p.173.

20. M.R. Nadler and C.P. Kempter: J.Phys.Chem. 1960, vol.64, p.1468.

21. T. Takei: Sci.Rep. Tohoku Univ., 1928, vol.17, p.939.

22. G.A. Geach and F.O. Jones: Plansee Proc. 1955, p.80.

23. E. Friedrich and L. Sittig: Z.anorg.allg. Chemie 1925, vol.144, p. 169.

24. C. Agte and H. Alterthum: Z.Techn.Phys., 1930, vol.11, p. 182.

25. V.N. Eremenko and T.Y. Velikanova: Poroshkovaya Metallurgiya, 1965, No.1, vol.25, p.41.

26. E. Rudy, St. Windisch, and Y.A. Chang: Technical Report AFML-TR-65-2, Part I, vol. 1 (Jan. 1965). DDC File Nr. AD-463-558.

27. M. Pirani and H. Alterthum: Z. Elektrochem, 1923, vol.29, p.5.

28. E. Rudy and G. Progulski: AFML-TR-65-2, Part III, Vol. II (Sept. 1966), Planseeber, Pulvermet (in print).

29. E. Rudy, R. Taylor, and T. Eckert: (in preparation for print).

30. W.E. Few and G.K. Manning: J.Metals 1942, vol.4, p.271.

31. L.B. Pankratz, W.W. Weller, and E. G. King: U.S. Bureau Mines, Rept. of Invest. 6861, 1966.

32. F. Bloch: Z. Physik, 1930, vol.61, p.607.

33. N. Terao: Jap.J.Appl. Phys. 1964, vol.3, p. 104.

34. E. Rudy and C.E. Brukl: J.Amer.Ceram.Soc. (in print).

35. E. Rudy, St. Windisch, and J.R. Hoffman: Technical Report AFML TR-65-2, Part I, Vol. VI (Jan 1966).

36. L.N. Butorina and Z.G. Pinsker: Soviet Physics, Crystallography, 1960, vol.5, p.560.

37. J.C. Slater, Introduction to Chemical Physics (McGraw-Hill, New York, 1939).

38. F.W.Vahldiek, S.A. Mersol, and C.T. Lynch: Techn.Report AFML-TR-66-268, August 1966.

DOCUMENT CONTROL DATA - R&D

(Security classification of title, body of abstract and indexing annotation must be entered when the overall report is classified)

1. ORIGINATING ACTIVITY *(Corporate author)* Materials Research Laboratory Aerojet-General Corporation Sacramento, California	2a. REPORT SECURITY CLASSIFICATION UNCLASSIFIED 2b. GROUP N.A.

3. REPORT TITLE

Ternary Phase Equilibrium in Transition Metal-Boron-Carbon-Silicon Systems. Part I. Related Binary Systems, Volume XI. Final Report on the Mo-C System

4. DESCRIPTIVE NOTES *(Type of report and inclusive dates)*

Documentary Report

5. AUTHOR(S) *(Last name, first name, initial)*

Rudy, E.
Windisch, St.
Stosick, A.J., and Hoffman, J.R.

6. REPORT DATE	7a. TOTAL NO. OF PAGES	7b. NO. OF REFS
April 1967	68	38

8a. CONTRACT OR GRANT NO.	9a. ORIGINATOR'S REPORT NUMBER(S)
AF 33(615)-1249	AFML-TR-65-2
b. PROJECT NO. 7350	[redacted]
c. Task No. 735001	9b. OTHER REPORT NO(S) *(Any other numbers that may be assigned this report)*
d.	

10. AVAILABILITY/LIMITATION NOTICES This document is subject to special export controls, and each transmittal to foreign governments or foreign nationals may be made only with prior approval of Metals & Ceramics Div., AF Materials Laboratory, Wright-Patterson Air Force Base, Ohio.

11. SUPPLEMENTARY NOTES	12. SPONSORING MILITARY ACTIVITY
	AFML (MAMC) Wright-Patterson AFB, Ohio 45433

13. ABSTRACT

The binary alloy system molybdenum-carbon was investigated by means of X-ray, metallographic, thermoanalytical, and melting point techniques on chemically analyzed specimens. The system (Figure 39) is characterized by three congruently melting, intermediate phases, Mo_2C, η-MoC_{1-x}, and α-MoC_{1-x}, of which only Mo_2C is stable at temperatures below 1650°C. Substoichiometric (<32.5 At% C) dimolybdenum carbide undergoes a homogeneous sublattice order-disorder transformation at temperatures of approximately 1400°C, whereas hyperstoichiometric compositions undergo a discontinuous phase-change. The order-disorder transitions in the Me_2C phases are discussed in terms of the structural changes involved in the transformation processes and the absence of long range sublattice coherency in stoichiometric or hyperstoichiometric compositions attributed to the impossibility of obtaining long range order in a linear chain of alternating carbon atoms and vacancies.

From the experimental phase relationships and the known thermodynamic data for Mo_2C, limits for the free energies of formation for the high temperature phases η-MoC_{1-x} and α-MoC_{1-x} are derived and found to be in good agreement with data previously obtained from phase equilibria in ternary metal-carbon systems.

This abstract is subject to special export controls, and each transmittal to foreign governments or foreign nationals may be made with prior approval of the Metals and Ceramics Division, AF Materials Laboratory, Wright-Patterson AFB Ohio 45433

DD FORM 1 JAN 64 1473

UNCLASSIFIED
Security Classification

UNCLASSIFIED

Security Classification

14. KEY WORDS	LINK A		LINK B		LINK C	
	ROLE	WT	ROLE	WT	ROLE	WT
Phase Equilibria Molybdenum-Carbon						

INSTRUCTIONS

1. ORIGINATING ACTIVITY: Enter the name and address of the contractor, subcontractor, grantee, Department of Defense activity or other organization *(corporate author)* issuing the report.

2a. REPORT SECURITY CLASSIFICATION: Enter the overall security classification of the report. Indicate whether "Restricted Data" is included. Marking is to be in accordance with appropriate security regulations.

2b. GROUP: Automatic downgrading is specified in DoD Directive 5200.10 and Armed Forces Industrial Manual. Enter the group number. Also, when applicable, show that optional markings have been used for Group 3 and Group 4 as authorized.

3. REPORT TITLE: Enter the complete report title in all capital letters. Titles in all cases should be unclassified. If a meaningful title cannot be selected without classification, show title classification in all capitals in parenthesis immediately following the title.

4. DESCRIPTIVE NOTES: If appropriate, enter the type of report, e.g., interim, progress, summary, annual, or final. Give the inclusive dates when a specific reporting period is covered.

5. AUTHOR(S): Enter the name(s) of author(s) as shown on or in the report. Enter last name, first name, middle initial. If military, show rank and branch of service. The name of the principal author is an absolute minimum requirement.

6. REPORT DATE: Enter the date of the report as day, month, year, or month, year. If more than one date appears on the report, use date of publication.

7a. TOTAL NUMBER OF PAGES: The total page count should follow normal pagination procedures, i.e., enter the number of pages containing information.

7b. NUMBER OF REFERENCES: Enter the total number of references cited in the report.

8a. CONTRACT OR GRANT NUMBER: If appropriate, enter the applicable number of the contract or grant under which the report was written.

8b, 8c, & 8d. PROJECT NUMBER: Enter the appropriate military department identification, such as project number, subproject number, system numbers, task number, etc.

9a. ORIGINATOR'S REPORT NUMBER(S): Enter the official report number by which the document will be identified and controlled by the originating activity. This number must be unique to this report.

9b. OTHER REPORT NUMBER(S): If the report has been assigned any other report numbers *(either by the originator or by the sponsor)*, also enter this number(s).

10. AVAILABILITY/LIMITATION NOTICES: Enter any limitations on further dissemination of the report, other than those imposed by security classification, using standard statements such as:

(1) "Qualified requesters may obtain copies of this report from DDC."

(2) "Foreign announcement and dissemination of this report by DDC is not authorized."

(3) "U. S. Government agencies may obtain copies of this report directly from DDC. Other qualified DDC users shall request through

_____."

(4) "U. S. military agencies may obtain copies of this report directly from DDC. Other qualified users shall request through

_____."

(5) "All distribution of this report is controlled. Qualified DDC users shall request through

_____."

If the report has been furnished to the Office of Technical Services, Department of Commerce, for sale to the public, indicate this fact and enter the price, if known.

11. SUPPLEMENTARY NOTES: Use for additional explanatory notes.

12. SPONSORING MILITARY ACTIVITY: Enter the name of the departmental project office or laboratory sponsoring *(paying for)* the research and development. Include address.

13. ABSTRACT: Enter an abstract giving a brief and factual summary of the document indicative of the report, even though it may also appear elsewhere in the body of the technical report. If additional space is required, a continuation sheet shall be attached.

It is highly desirable that the abstract of classified reports be unclassified. Each paragraph of the abstract shall end with an indication of the military security classification of the information in the paragraph, represented as *(TS), (S), (C), or (U)*.

There is no limitation on the length of the abstract. However, the suggested length is from 150 to 225 words.

14. KEY WORDS: Key words are technically meaningful terms or short phrases that characterize a report and may be used as index entries for cataloging the report. Key words must be selected so that no security classification is required. Identifiers, such as equipment model designation, trade name, military project code name, geographic location, may be used as key words but will be followed by an indication of technical context. The assignment of links, rules, and weights is optional.

UNCLASSIFIED

Security Classification